NAVAL POSTGRADUATE SCHOOL

MONTEREY, CALIFORNIA

THESIS

FUEL OPTIMAL LOW THRUST TRAJECTORIES FOR AN ASTEROID SAMPLE RETURN MISSION

by

Jack W. Rust

March 2005

Thesis Advisor:	I. Michael Ross
Second Reader:	Stacy Weinstein

THIS PAGE INTENTIONALLY LEFT BLANK

REPORT DOCUMENTATION PAGE			*Form Approved OMB No. 0704-0188*
Public reporting burden for this collection of information is estimated to average 1 hour per response, including the time for reviewing instruction, searching existing data sources, gathering and maintaining the data needed, and completing and reviewing the collection of information. Send comments regarding this burden estimate or any other aspect of this collection of information, including suggestions for reducing this burden, to Washington headquarters Services, Directorate for Information Operations and Reports, 1215 Jefferson Davis Highway, Suite 1204, Arlington, VA 22202-4302, and to the Office of Management and Budget, Paperwork Reduction Project (0704-0188) Washington DC 20503.			
1. AGENCY USE ONLY *(Leave blank)*	2. REPORT DATE March 2005	3. REPORT TYPE AND DATES COVERED Master's Thesis	
4. TITLE AND SUBTITLE: Fuel Optimal Low Thrust Trajectories for an Asteroid Sample Return Mission		5. FUNDING NUMBERS	
6. AUTHOR(S) Rust, Jack W.			
7. PERFORMING ORGANIZATION NAME(S) AND ADDRESS(ES) Naval Postgraduate School Monterey, CA 93943-5000		8. PERFORMING ORGANIZATION REPORT NUMBER	
9. SPONSORING /MONITORING AGENCY NAME(S) AND ADDRESS(ES) Jet Propulsion Laboratory 4800 Oak Grove Drive Pasadena, CA 91109-8099		10. SPONSORING/MONITORING AGENCY REPORT NUMBER	
11. SUPPLEMENTARY NOTES The views expressed in this thesis are those of the author and do not reflect the official policy or position of the Department of Defense or the U.S. Government.			
12a. DISTRIBUTION / AVAILABILITY STATEMENT Approved for public release; distribution is unlimited		12b. DISTRIBUTION CODE	

13. ABSTRACT (maximum 200 words)

This thesis explores how an Asteroid Sample Return Mission might make use of solar electric propulsion to send a spacecraft on a journey to the asteroid 1989ML and back. It examines different trajectories that can be used to get an asteroid sample return or similar spacecraft to an interplanetary destination and back in the most fuel-efficient manner. While current plans call for keeping such a spacecraft on the asteroid performing science experiments for approximately 90 days, it is prudent to inquire how lengthening or shortening this time period may affect mission fuel requirements. Using optimal control methods, various mission scenarios have been modeled and simulated. The results suggest that the amount of time that the spacecraft may spend on the asteroid surface can be approximated as a linear function of the available fuel mass. Furthermore, It can be shown that as maximum available thrust is decreased, the radial component of the optimal thrust vector becomes more pronounced.

14. SUBJECT TERMS Low Thrust, Solar Electric Propulsion, Optimal Design, Trajectory Design, Ion Thruster, Asteroid Rendezvous	15. NUMBER OF PAGES 75
	16. PRICE CODE

17. SECURITY CLASSIFICATION OF REPORT	18. SECURITY CLASSIFICATION OF THIS PAGE	19. SECURITY CLASSIFICATION OF ABSTRACT	20. LIMITATION OF ABSTRACT
Unclassified	Unclassified	Unclassified	UL

NSN 7540-01-280-5500

Standard Form 298 (Rev. 2-89)
Prescribed by ANSI Std. 239-18

THIS PAGE INTENTIONALLY LEFT BLANK

Approved for public release; distribution is unlimited

FUEL OPTIMAL LOW THRUST TRAJECTORIES FOR AN ASTEROID SAMPLE RETURN MISSION

Jack W. Rust
Lieutenant Commander, United States Navy
B.S., University of Arizona, 1994

Submitted in partial fulfillment of the
requirements for the degree of

MASTER OF SCIENCE IN ASTRONAUTICAL ENGINEERING

from the

NAVAL POSTGRADUATE SCHOOL
March 2005

Author: Jack W. Rust

Approved by: I. Michael Ross
Thesis Advisor

Stacy Weinstein
Second Reader

Anthony J. Healey
Chairman, Department of Mechanical and
Astronautical Engineering

THIS PAGE INTENTIONALLY LEFT BLANK

ABSTRACT

This thesis explores how an Asteroid Sample Return Mission might make use of solar electric propulsion to send a spacecraft on a journey to the asteroid 1989ML and back. It examines different trajectories that can be used to get an asteroid sample return or similar spacecraft to an interplanetary destination and back in the most fuel-efficient manner. While current plans call for keeping such a spacecraft on the asteroid performing science experiments for approximately 90 days, it is prudent to inquire how lengthening or shortening this time period may affect mission fuel requirements. Using optimal control methods, various mission scenarios have been modeled and simulated. The results suggest that the amount of time that the spacecraft may spend on the asteroid surface can be approximated as a linear function of the available fuel mass. Furthermore, It can be shown that as maximum available thrust is decreased, the radial component of the optimal thrust vector becomes more pronounced.

THIS PAGE INTENTIONALLY LEFT BLANK

TABLE OF CONTENTS

THIS PAGE INTENTIONALLY LEFT BLANK

LIST OF FIGURES

LIST OF TABLES

THIS PAGE INTENTIONALLY LEFT BLANK

ACKNOWLEDGMENTS

This effort would not have been possible without the patient support and untiring devotion of my loving wife, Connie, and my daughter, Jennifer.

Nor could it have succeeded without the cooperation and expertise of the many people who make up JPL's Navigation and Mission Design Section. I am particularly indebted to Carl Sauer, Mike Lisano, Roby Wilson, Steven Williams, Jon Sims, Edward Rinderle, Shyam Baskaran, and Elliot Cutting. All of whom were exceedingly generous with both their time and their knowledge.

Finally, I would like to thank Professor Mike Ross for teaching me more than I ever thought I could learn about optimal control theory; and, Stacy Weinstein for making me feel as though I were actually a part of that exceptional team of space professionals that make up The Jet Propulsion Laboratory.

THIS PAGE INTENTIONALLY LEFT BLANK

I. INTRODUCTION

A. THE HISTORICAL PERSPECTIVE

It is frequently asserted that the history of modern space propulsion began with the invention of gunpowder in China over a thousand years ago. It is around this time that the first solid fuel chemical rockets appeared. Even with the later development of liquid fueled rockets and space launch vehicles in the Twentieth Century, many of the fundamental principles that govern the construction and operation of modern rocket propulsion systems have changed little since the time when ancient Chinese rocket engineers like the legendary Wan Hoo are said to have attempted the first space flight using a rocket propelled wicker chair. Those present for the occasion, and prudent enough to have stood well clear of the would be astronaut, were among the first to fully understand and appreciate the tremendous unwieldy power and volatility of the rocket, to say nothing of the difficulties inherent in applying any form of control to the process of thrusting [Ref. 14]. A similar understanding of rockets combined with healthy respect for their limitations has persisted down the centuries and continues to inform every aspect of space propulsion engineering to this day.

In spite of the risks, rockets continue to be the preferred method of primary propulsion. Understandable, since a considerable part of any modern day space mission involves simply getting into orbit. Rocket propulsion works in the Earth's atmosphere more or less as well as it does in space. Moreover, it can be tested and developed here on Earth without the use of expensive vacuum chambers. Given the fledgling state of current space fairing capability, chemical rocket propulsion makes perfect sense.

In the near future however, space mission planning is increasingly likely to begin not at launch, but with a highly maneuverable spacecraft already placed in orbit. Mission planning, to the extent that it occurs prior to launch, is likely to be open ended with specific trajectories left undefined until the need arises. In many instances, the inherent risks and inefficiencies of the chemical rocket will make it

an unattractive alternative for primary propulsion. Space propulsion systems of the future will combine unprecedented efficiency with a degree of reliability, flexibility, and control not seen in modern chemical rockets. Designed to function only in the vacuum of space, their impact on exploration is likely to be as profound as that of the innovations in sailing technology that preceded the Sixteenth Century voyages of discovery.

B. THE EMERGENCE OF ION PROPULSION

In October of 1998, a spacecraft called Deep Space One was launched from Cape Canaveral. Its primary mission was to test a number of high-risk technologies. Foremost among these was the Boeing NSTAR 30 cm gridded ion thruster. Though ion thrusters had been around for decades, Deep Space One was the first spacecraft to successfully employ an ion thruster for primary propulsion on an extended deep space mission [Ref. 12].

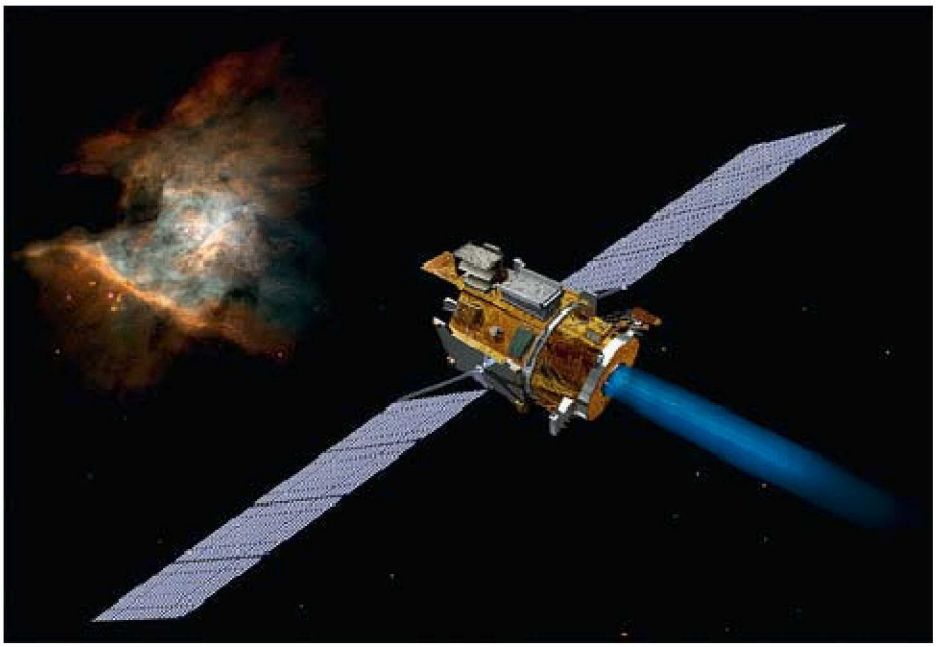

Figure 1. Deep Space One [From: Ref. 1]

Over the next three years, NSTAR would perform flawlessly over 16,000 hours of continuous operation [Ref. 1]. Since then, the European Space Agency has also successfully employed an ion thruster to propel Europe's first lunar mission, known as SMART 1, into orbit around the moon. Having proven itself to

be a safe, effective, and reliable engine for primary propulsion, the ion thruster is presently being integrated into many spacecraft now under development.

Ion thrusters work by using electricity to ionize an inert gas such as xenon and accelerate it out of the spacecraft at extremely high velocity. While actual thrust is imperceptibly low when compared to chemical rockets, ion thrusters are capable of applying this thrust continuously for months at a time. Fuel mass efficiency, as measured in terms of specific impulse, can be more than ten times higher than that of chemical rockets.

While a spacecraft thus propelled can frequently take much longer to reach a particular destination than a conventional chemical rocket, it need only carry a small fraction of the chemical thrusters' required fuel mass, thus leaving more room for additional payload. Moreover, an ion thruster employs no moving parts and uses a chemically inert propellant. Energy is not stored in the form of volatile chemical explosives but is extracted from the environment through the spacecraft's solar panels. This approach gives the ion thruster a tremendous safety advantage over chemical thrusters.

C. A PROBLEM WELL SUITED TO OPTIMAL CONTROL

In addition to these advantages, ion thrusters are much easier to control than chemical thrusters. On a fundamental level a chemical thruster propels a spacecraft by applying a series of prolonged explosions. The effect on spacecraft trajectory cannot always be precisely predicted and this uncertainty must be accounted for in the planning of spacecraft maneuvers. Uneven burning of solid propellants frequently necessitates spin stabilization of the entire spacecraft while a burn is underway. Throttling or shutting down a solid booster before all the fuel is exhausted is impracticable. Liquid chemical thrusters can be throttled, shutdown, and restarted. But the repeated cycling of valves over time can contribute to increasingly uncertain performance in the long term.

Ion thrusters, on the other hand, can be throttled up and down to the nearest thousandth of a Newton merely by changing the applied electrical power. While thruster grid erosion can result in slight performance degradation over

time, the absence of moving parts enhances reliability and ensures predictable performance over the life of the spacecraft. Lengthy burn times equate to long reaction and recovery times that facilitate timely intervention if thrusting is not having the desired effect on spacecraft trajectory. Moreover, thruster pointing is easily accomplished with conventional momentum wheels or gimbaled mountings even while thrusting is at maximum power.

Such enhanced control and flexibility facilitates a wide variety of useful tasks including precise maneuvering for rendezvous and surveillance of asteroids or other spacecraft. It makes docking for servicing, refueling, and repair much safer and easier to control and automate. It also makes possible the kind of precise formation flying necessary for sparse aperture remote sensing using multiple spacecraft.

Enhanced controllability naturally translates into greater opportunity to exercise optimal control. Spacecraft trajectories can be designed to minimize transit time, minimize fuel consumption, maximize precision, or optimize some other desired mission parameter. Trajectories can even be designed to optimize a precisely defined combination of parameters in a precisely defined way - a problem that naturally lends itself to real time computerized automation.

D. THE FUTURE OF SPACE PROPULSION

Not surprisingly, government organizations and private companies from around the world are even now developing and marketing ion propulsion spacecraft to fill a wide variety of roles and missions. In the UK, the recently privatized consortium of Defense Ministry laboratories known as Qinetiq PLC is marketing a line of highly maneuverable microsatellites to provide space situational awareness to its customers including the ability to rendezvous with and photograph other spacecraft in geosynchronous orbit. The spacecraft weighs less than two hundred kilograms and uses a single ion thruster for primary propulsion [Ref. 2].

Also in Europe, Orbital Recovery Corporation is marketing the ConeXpress Orbital Life Extension Vehicle (CX OLEV) as an ion propulsion

"space tug" to facilitate the refueling and servicing of communications satellites that have expended their onboard propellant supplies but are otherwise quite functional, thereby giving a new lease on life to a very expensive capital investment. The company foresees a large market among the global telecommunications industry. In a stroke of innovative engineering, the spacecraft structure actually doubles as the Ariane V payload adapter; thus, preserving valuable payload volume for paying customers [Ref. 3].

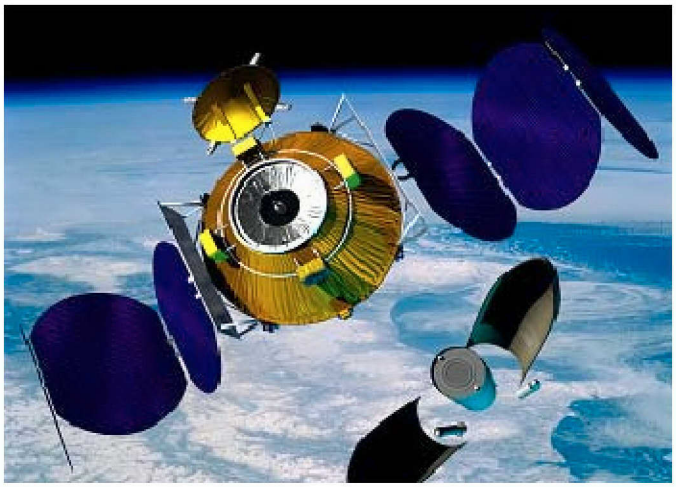

Figure 2. ConeXpress Orbital Life Extension Vehicle [From: Ref. 3]

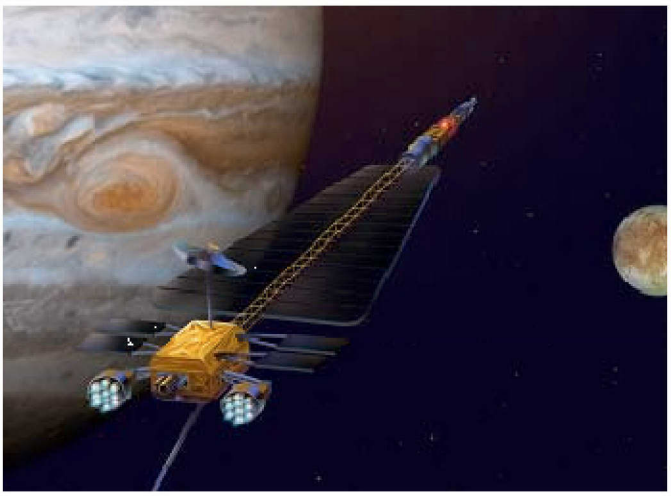

Figure 3. Jupiter Icy Moons Orbiter [From: Ref. 4]

Large arrays of ion thrusters are envisioned as the primary propulsion system for NASA's Jupiter Icy Moons Mission. Power is to be provided by an onboard nuclear reactor under development as part of NASA's Project Prometheus [Ref. 4].

In the near term, NASA is proposing a number of smaller deep space missions to be propelled by ion thrusters. An asteroid sample return mission, the subject of this thesis, is one of these. But there should be no doubt that the utility and applicability of the ideas discussed here in the context of the asteroid sample return mission extend well beyond any single spacecraft or any single type of mission. Whether for military, commercial, or purely scientific purposes, optimal control of low thrust trajectories is likely to become an increasingly important aspect of space mission planning in the years ahead.

II. BACKGROUND

A. THE ASTEROID SAMPLE RETURN MISSION

The Near Earth Asteroid Sample Return Mission is intended to provide planetary geologists an opportunity to examine asteroid mineral samples up close for the first time. In February 2001, the NEAR spacecraft successfully landed on the asteroid Eros and provided detailed data on chemical and mineral composition as well as numerous close up photographs of the asteroid's surface features. While this kind of information can be of immense value in answering fundamental questions about the nature of the solar system, actual samples of asteroid surface material could yield still greater discoveries by allowing scientists to test the material back on Earth [Ref. 5].

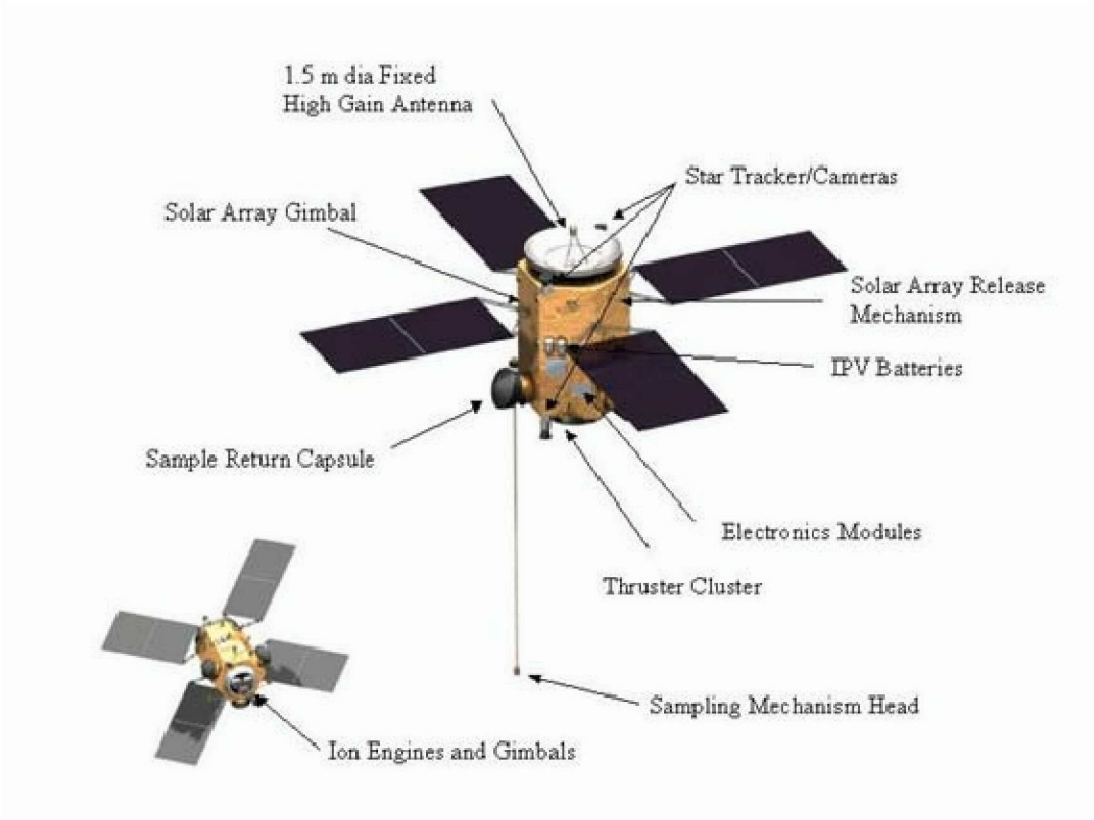

Figure 4. Reference Sample Return Spacecraft [From Ref. 5]

B. TARGET AND TRAJECTORY

Asteroid 1989ML is the reference mission destination for this thesis. But among the hundreds of possibilities, there are many attractive candidates. So much so that a multiple asteroid rendezvous has been considered. Deciding on which bodies to visit and in what sequence is itself a difficult optimization problem [Ref. 17].

Figure 5 below shows two circles approximating the orbit of the Earth (blue) and Mars (red) based on their semi-major axes. 1989ML is roughly one kilometer across and lies in a slightly eccentric orbit (green) between the two.

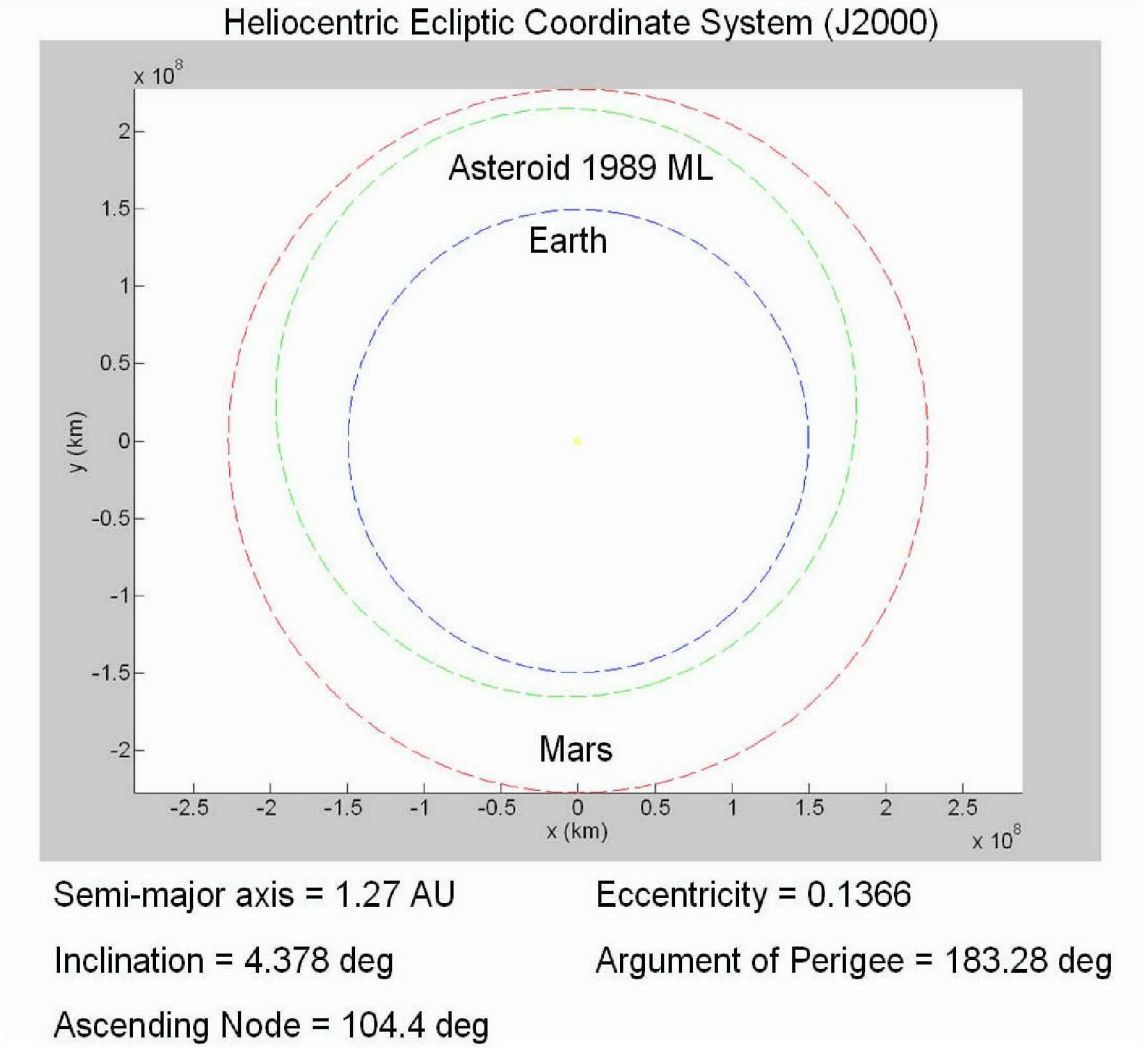

Figure 5. 1989 ML Orbit Diagram

C. THE ASTEROID SAMPLE RETURN SPACECRAFT

The requirement to actually fly out to the asteroid and return poses a number of technical challenges beyond those encountered in a one way journey such as that undertaken by NEAR in 2001. Spacecraft mass becomes an even more critical issue since the spacecraft must now carry sufficient fuel for a round trip. The mission can be expected to last at least twice as long, thus mandating high component reliability and reduced risk, qualities not frequently associated with pressurized tankage, valves, and piping systems. The target asteroid, 1989ML, being less than one kilometer in diameter, exerts very little gravitational pull. Precise maneuvering in such a weak gravity field necessitates a very fine level of thrust control. The ion thruster favorably addresses all of these issues and is thus particularly well suited to fulfill the primary propulsion requirements for this mission. The reference mission uses three NSTAR ion thrusters; two for propulsion and one spare. Each thruster will be similar to the one flown for the first time on Deep Space One.

THIS PAGE INTENTIONALLY LEFT BLANK

III. FORMULATING THE ASTEROID SAMPLE RETURN PROBLEM

A. MODELING THE DYNAMICS

1. Two Dimensional Model

Since the orbital inclination of 1989ML is only 4.38 degrees, the sample return mission can be modeled two dimensionally using the small angle approximation. This greatly simplifies the calculations while still yielding reasonably accurate results. [Ref. 7]

2. Coordinate System, State Vector, and Control Vector

The two dimensional model naturally lends itself to a heliocentric polar coordinate system in which the spacecraft state vector can be described in terms of radial position r, angular displacement with respect to Aries θ, radial velocity u, transverse velocity v, and spacecraft mass m:

$$\underline{x} = \begin{bmatrix} r \\ \theta \\ u \\ v \\ m \end{bmatrix} \qquad (3.1)$$

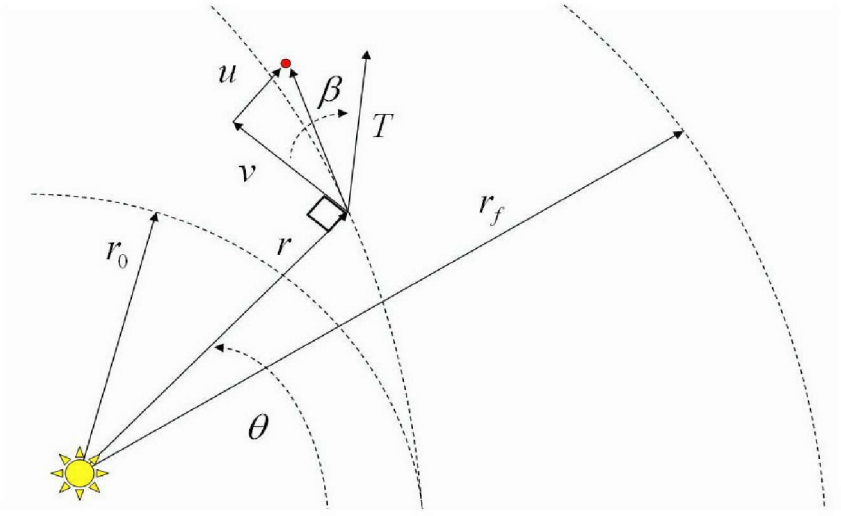

Figure 6. Polar Coordinate System

Control is accomplished by means of varying the magnitude and direction of spacecraft thrust,

$$\underline{u} = \begin{bmatrix} T \\ \beta \end{bmatrix} \qquad (3.2)$$

Thrust magnitude T is constrained consistent with rated maximum thrust and the number of working thrusters. Control of thrust direction β is constrained in such a way as to reflect the full 360 degree range of motion afforded by slewing the entire spacecraft.

$$0 \le T \le 2 \times \left(92 \times 10^{-3} N\right)$$

$$0 \le \beta \le 2\pi$$

3. Dynamic Equations

The dynamic equations used to model the reference mission trajectory are based on a heliocentric two body model [Refs. 8, 9] and can be derived using LaGrangian mechanics as follows.

$$\frac{d}{dt}\left(\frac{\partial L}{\partial \dot{\vec{x}}}\right) - \frac{\partial L}{\partial \vec{x}} = Q_{NC}^{T}$$

in which Q_{NC}^{T} is the generalized non-conservative force vector representing spacecraft thrust. System kinetic and potential energy terms define the LaGrangean,

$$T = \frac{1}{2}\vec{V} \cdot \vec{V} = \frac{1}{2}(\dot{r}^2 + r^2\dot{\theta}^2)$$

$$V = \frac{-GM}{r} = -\frac{\mu}{r}$$

$$L = T - V = \frac{1}{2}(\dot{r}^2 + r^2\dot{\theta}^2) + \frac{\mu}{r}$$

Spacecraft acceleration (thrust divided by mass) is described in polar coordinates,

$$a = \frac{T}{m}$$

$$\vec{a} = a\cos\beta\hat{\theta} + a\sin\beta\hat{r}$$

$$a_\theta = \frac{T}{m}\cos\beta \qquad\qquad a_r = \frac{T}{m}\sin\beta$$

Generalized specific non-conservative force and torque vectors, in the radial and angular direction respectively, can then be defined as,

$$Q_r = a\sin\beta \qquad\qquad Q_\theta = ra\cos\beta$$

and applied to derive the dynamic equations such that,

$$\frac{d}{dt}\left(\frac{\partial L}{\partial \dot{r}}\right) - \frac{\partial L}{\partial r} = Q_r \qquad\qquad \frac{d}{dt}\left(\frac{\partial L}{\partial \dot{\theta}}\right) - \frac{\partial L}{\partial \theta} = Q_\theta$$

in which,

$$\frac{d}{dt}\left(\frac{\partial L}{\partial \dot{r}}\right) = \ddot{r} \qquad\qquad \frac{d}{dt}\left(\frac{\partial L}{\partial \dot{\theta}}\right) = 2r\dot{r}\dot{\theta} + r^2\ddot{\theta}$$

$$\frac{\partial L}{\partial r} = r\dot{\theta}^2 - \frac{\mu}{r^2} \qquad\qquad \frac{\partial L}{\partial \theta} = 0$$

and,

$$v = r\dot{\theta} \qquad\qquad v = r\dot{\theta}$$
$$\dot{u} = \ddot{r} \qquad\qquad \dot{v} = r\ddot{\theta} + \dot{r}\dot{\theta}$$

such that,

$$\ddot{r} - r\dot{\theta}^2 + \frac{\mu}{r^2} = a\sin\beta \qquad\qquad 2r\dot{r}\dot{\theta} + r^2\ddot{\theta} = ra\cos\beta$$

$$\dot{u} - \frac{v^2}{r} + \frac{\mu}{r^2} = a\sin\beta \qquad\qquad \dot{v} + \frac{uv}{r} = a\cos\beta$$

$$\dot{u} = \frac{v^2}{r} - \frac{\mu}{r^2} + a\sin\beta \qquad\qquad \dot{v} = a\cos\beta - \frac{uv}{r}$$

which results in dynamic equations that fully describe the two body heliocentric model,

$$\underline{\dot{x}} = \begin{bmatrix} \dot{r} \\ \dot{\theta} \\ \dot{u} \\ \dot{v} \\ \dot{m} \end{bmatrix} = f = \begin{bmatrix} u \\ \frac{v}{r} \\ \frac{v^2}{r} - \frac{\mu}{r^2} + \frac{T}{m}\sin\beta \\ \frac{-uv}{r} + \frac{T}{m}\cos\beta \\ \frac{-T}{V_e} \end{bmatrix} \quad (0.1)$$

where V_e is thruster exhaust velocity and μ is the solar gravitational constant. The gravitational effects of planets and asteroids can be neglected for the purposes of this simplified model without substantially affecting the outcome of the results. [Ref. 9]

B. MODELING THE EVENTS

To generate an optimal trajectory, it is first necessary to specify initial and final events, denoted by e, in terms of the five variables comprising the spacecraft state vector at any given point. Wherever this can not be done explicitly, an orbital element or other quantity must be calculated from the state variables. This element or quantity can then be constrained to correspond to the requirements of a particular event. Physically, these events represent launch from Earth, e_0, the landing on 1989ML , e_{left}, departure from 1989ML , e_{right}, and subsequent return to Earth , e_f :

$$e_0 = \begin{bmatrix} r_0 \\ \theta_0 \\ u_0 \\ v_0 \\ C3_{used} \\ m_0 \end{bmatrix} \quad e_{left} = \begin{bmatrix} m_{left} \\ a_{left} \\ e_{left} \\ \tilde{\omega}_{left} \\ t_{left} \\ M_{left} \end{bmatrix} \quad e_{right} = \begin{bmatrix} m_{right} \\ a_{right} \\ e_{right} \\ \tilde{\omega}_{right} \\ t_{right} \\ M_{right} \end{bmatrix} \quad e_f = \begin{bmatrix} r_f \\ M_f \\ u_f \\ v_f \\ V_{HE} \end{bmatrix} \quad (0.2)$$

It should be noted that the bold letter $\boldsymbol{e}$ denotes an event condition including all of its corresponding elements as shown above. Whereas the ordinary e simply denotes orbital eccentricity at a particular event. r,θ,u,v and m are state variables and are subscripted above to denote their value at a particular event.

C3 is traditionally taken to be the major performance parameter agreed on between the launch vehicle system and the planetary spacecraft [Ref. 10]. The injected mass or payload mass for a given launch vehicle and a given trajectory is always a function of C3. In other words, the spacecraft wet mass is dictated by C3. In this case, C3 equals the square of the hyperbolic excess velocity of the spacecraft with respect to Earth at the initial event, and constitutes the launch energy required to get to 1989ML using the given trajectory. It is therefore necessary to constrain C3 within the performance parameters of the booster as part of the initial event constraints.

V_{HE} signifies final hyperbolic excess velocity with respect to Earth at the final event. a represents the semi-major axis of the spacecraft orbit at a particular event. ω is the argument of periapsis (measured from the Ascending Node), $\tilde{\omega}$ is the longitude of periapsis (measured from the Vernal Equinox), t is the time, and M is the mean anomaly corresponding to a particular event.

The time between the two interior events is spent on the asteroid surface and the spacecraft trajectory is assumed to be identical to that of the asteroid. Thus, it is not subject to optimization. A MATLAB application package called DIDO is used throughout this work to generate optimal trajectories based on the specified dynamics, events, and constraints.

1. Initial Events

For the purposes of this simplified analysis, the Earth's orbit around the Sun is assumed to be perfectly circular with a radius of 1 Astronomical Unit or 1 AU (approximately $1.495\times10^{6}km$). The initial spacecraft radial position is thus specified at 1 AU, but initial angular displacement is completely unconstrained leaving DIDO to choose the optimum angular position, and thus the

corresponding calendar date, from which to launch in order to minimize fuel consumption consistent with mission constraints. Spacecraft wet mass can be specified at the beginning of any scenario. This mass is then used as the initial value for the corresponding state variable.

Maximum C3 can also be specified at the beginning of each scenario. DIDO will choose an initial spacecraft velocity vector so as to minimize ion thruster fuel consumption within the constraints of the maximum C3 specified. Initial event constraints are summarized below.

$$r_0 = r_{earth}$$
$$0 < \upsilon_0 \le 2\pi$$
$$-\sqrt{C3_{\max}} \le u_0 \le \sqrt{C3_{\max}}$$
$$-\sqrt{C3_{\max}} \le v_0 \le \sqrt{C3_{\max}}$$
$$0 \le C3_{used} \le C3_{\max}$$
$$m_0 = m_{wet}$$

In order to constrain C3 within the maximum C3 specified at the beginning of the simulation, it is first necessary to define C3 in terms of the spacecraft state variables. The magnitude of the initial spacecraft velocity (in scaled units or km/sec) is given by equation 3.5.

$$V_0 = \sqrt{u_0^2 + v_0^2} \qquad (3.5)$$

Initial flight path angle is given by equation 3.6.

$$fpa_0 = \arctan(u_0 / v_0) \qquad (3.6)$$

These terms are employed in equation 3.7 [Ref. 10] through which the spacecraft state vector can be constrained consistent with a specified maximum C3.

$$C3 = V_{earth}^2 + V_0^2 - 2V_{earth}V_0\cos(fpa_0) \quad (3.7)$$

2. Interior Events

Between the time that the spacecraft touches down on 1989ML and the time it lifts off, the spacecraft state variables representing position and velocity

will change consistent with the orbit of 1989ML. Since the asteroid's semi-major axis, eccentricity, and longitude of periapsis remain constant throughout the orbit, these quantities are calculated in terms of the spacecraft state variables and then constrained to equal the corresponding values for 1989ML. This effectively collocates the spacecraft with 1989ML for the surface time specified at the beginning of a simulation. Since a primary motivation for this thesis is to determine whether or not changes in asteroid surface time can be used to reap significant savings in fuel mass, it is desirable to run different mission scenarios in which various asteroid surface times can be imposed.

For a circular orbit, angular displacement is directly proportional to elapsed time. For elliptical orbits, mean anomaly is directly proportional to elapsed time. Thus, changes in mean anomaly are used here to solve for and constrain asteroid surface time within a specified window [Ref. 18].

To find mean anomaly in terms of the state variables using Kepler's Equation, it is first necessary to calculate the semi-major axis, and eccentricity vector for the event in question. After converting spacecraft position and velocity into cartesion coordinates,

$$\vec{R} = \begin{bmatrix} r\cos\theta \\ r\sin\theta \\ 0 \end{bmatrix} \qquad \vec{V} = \begin{bmatrix} u\cos\theta - v\sin\theta \\ u\sin\theta - v\cos\theta \\ 0 \end{bmatrix}$$

Specific mechanical energy is found in terms of spacecraft orbital radius [Ref. 7].

$$\xi = \frac{\left|\vec{V}\right|^2}{2} - \frac{\mu}{r} \quad (3.8)$$

Semi-major axis is then calculated [Ref. 7].

$$a = -\frac{\mu}{2\xi} \quad (3.9)$$

Along with the eccentricity vector [Ref. 7].

$$\vec{e} = \frac{\left(V^2 - \frac{\mu}{r}\right)\vec{r} - \left(\vec{r} \cdot \vec{V}\right)\vec{V}}{\mu} \qquad (3.10)$$

Eccentric anomaly is then found using the arctangent of the following two expressions in which υ is the true anomaly [Ref. 7].

$$\sin E = \frac{\sin \upsilon \sqrt{1 - e^2}}{1 + \cos \upsilon} \qquad (3.11)$$

$$\cos E = \frac{ae + r \cos \upsilon}{a} \qquad (3.12)$$

which is all that is needed to solve for mean anomaly at asteroid arrival and asteroid departure using Kepler's Equation (Equation 3.14). Mean motion while on the asteroid is found using the semi-major axis and the solar gravitation constant in Equation 3.13.

$$n = \sqrt{\frac{\mu}{a^3}} \qquad (3.13)$$

$$M = E - e \sin E \qquad (3.14)$$

A corresponding time can thus be calculated for arrival or departure.

$$t = \frac{M}{n}$$

Longitude of periapsis can be found using Equation 3.15 [Ref. 7],

$$\cos\left(\tilde{\omega}\right) = \frac{\hat{I} \cdot \vec{e}}{\left|\hat{I}\right|\left|\vec{e}\right|} \qquad (3.15)$$

taking advantage of the small angle approximation, Equation 3.15 can be constrained such that,

$$\tilde{\omega} = \Omega + \omega$$

where the argument of periapsis of 1989ML is defined as $\omega = 183.28^0$ and the longitude of the ascending node for 1989ML is defined as $\Omega = 104.42^0$.

Finally, spacecraft mass at rendezvous is set equal to the spacecraft mass at departure since no thrusting should occur while the spacecraft is on the surface.

$$m_{left} = m_{right}$$

3. Final Events

Final spacecraft radius at Earth return must equal 1 AU since Earth orbit around the Sun is assumed to be perfectly circular. Once again, DIDO is free to pick final angular displacement, but subject to the constraint imposed by Earth asteroid phasing requirements. Thus, the angular position of Earth is moved forward from the initial launch position of the spacecraft in direct proportion to Earth mean motion and total flight time. The final spacecraft angular position is then constrained to this value such that,

$$\cos(M_{earth_{final}} - \theta_f) - 1 = 0$$

Unlike the rendezvous with 1989ML, in which spacecraft position and velocity are matched to the asteroid, Earth return can be characterized as an intercept in which some hyperbolic excess velocity (typically no more than 5 kilometers per second) is permitted. This value can be specified at the beginning of each simulation. DIDO allocates the specified magnitude among the transverse and radial components of the final state in an optimal fashion; shaping the trajectory to minimize ion thruster fuel consumption.

C. SIMPLIFIED MODEL OF SPACECRAFT AND THRUSTER

The spacecraft model used in the simulations featured here assumes a fully fueled or "wet" mass of 1222 kg and mounts three NSTAR thrusters; two of which are operated at any given time.

NSTAR Throttle Level	Mission Throttle Level	PPU Input Power (kW)	Engine Input Power (kW)	Measured Thrust (mN)	Main Flow Rate (sccm)	Cathode Flow Rate (sccm)	Neutralizer Flow Rate (sccm)	Specific Impulse (s)	Total Efficiency
12	85	1.99	1.86	75.34	19.99	2.91	2.82	3035	0.602
11	83	1.94	1.82	72.55	18.63	2.75	2.67	3125	0.610
11	83	1.96	1.83	72.63	18.62	2.75	2.67	3131	0.609
10	77	1.84	1.72	69.54	18.59	2.75	2.67	3000	0.594
10	76	1.82	1.70	67.21	17.31	2.58	2.51	3109	0.602
10	75	1.79	1.68	66.81	17.33	2.58	2.51	3087	0.601
10	74	1.77	1.66	66.11	17.33	2.59	2.51	3054	0.595
10	73	1.75	1.65	65.64	17.31	2.59	2.51	3035	0.594
10	72	1.73	1.63	65.15	17.31	2.59	2.51	3012	0.592
9	69	1.67	1.57	62.27	16.08	2.50	2.43	3070	0.597
6	48	1.29	1.22	47.43	11.42	2.50	2.42	3006	0.573
6	48	1.29	1.22	47.39	11.44	2.49	2.42	3004	0.571
3	27	0.89	0.84	31.70	6.93	2.50	2.43	2770	0.511
0	6	0.50	0.48	20.77	6.05	2.50	2.43	1961	0.418

Table 1. Flight Engine Performance Measured in Space [From Ref. 12]

To model the performance of the NSTAR ion thruster, values for Measured Thrust and corresponding Specific Impulse are selected or interpolated from Table 1. While the actual NSTAR thruster is capable of automatically switching between dozens of Mission Throttle Levels to accommodate the fluctuating availability of electrical power, the simplified model used here neglects to account for this feature; nor does it account for variations in solar flux levels as a function of distance from the Sun. Therefore, Specific Impulse and Maximum Thrust must be specified at the beginning of each simulation. During the simulation, spacecraft thrust ranges all the way from zero to the specified maximum thrust constraint while specific impulse remains constant at all times.

D. VALIDATING THE MODEL

1. Optimality

After a mission trajectory is generated, optimality can be verified using the basic principles of optimal control theory. The theory states that in order for a trajectory to be optimal, the Hamiltonian must equal zero at all points along the trajectory. Furthermore, the derivative of the LaGrangean of the Hamiltonian with respect to the individual controls should also be zero while fulfilling the requirements of the Complimentarity Condition [Ref. 8, 13].

The Hamiltonian of the dynamics described by equation 3.3 is defined such that:

$$H\left(\lambda,x,u,t\right)=F\left(x,u,t\right)+\lambda^{T}f\left(x,u,t\right) \qquad (3.16)$$

in which λ,x,u,t represent the costate, state, control, and time respectively. Here, optimality is defined only in terms of an endpoint cost - final spacecraft mass. Therefore, the first term in the right hand side of the equation equals zero. The second term is expanded to show all state and costate variables below.

$$H=\lambda_r u+\lambda_\upsilon\frac{v}{r}+\lambda_u\frac{v^2}{r}-\lambda_u\frac{\mu}{r^2}+\lambda_u\frac{T}{m}\sin\beta-\lambda_v\frac{uv}{r}+\lambda_v\frac{T}{m}\cos\beta-\lambda_m\frac{T}{V_e} \qquad (3.17)$$

Applying the Karush-Kuhn-Tucker (KKT) condition in which,

$$\frac{\partial\bar{H}}{\partial u}=\frac{\partial H}{\partial u}+\left(\frac{\partial H}{\partial u}\right)^{T}\mu=0$$

where the LaGrangian of the Hamiltonian can be defined as:

$$\bar{H}\left(\lambda,x,u,t,\mu\right)=H\left(\lambda,x,u,t\right)+\mu^{T}h\left(u,t\right) \qquad (3.18)$$

in which μ is the KKT multiplier and h is the constraint function [Ref. 13].and taking the derivative with respect to each control variable yields,

$$\frac{\partial\bar{H}}{\partial T}=\lambda_u\frac{1}{m}\sin\beta+\lambda_v\frac{1}{m}\cos\beta-\lambda_m\frac{1}{V_e}+\mu_T \qquad (3.19)$$

$$\frac{\partial\bar{H}}{\partial\beta}=\lambda_u\frac{T}{m}\cos\beta-\lambda_v\frac{T}{m}\sin\beta+\mu_\beta \qquad (3.20)$$

If in fact the generated trajectory is optimal, the Minimum Principle requires that the results of equations 3.17, 3.19, and 3.20 be close to zero at any point in the trajectory. While this does not assure optimality, a result substantially greater than zero usually proves that the solution is not optimal.

Further validation is provided by exploiting the Complementarity Condition [Ref. 13]. The KKT multiplier for each of the two control variables on the left in

Equations 3.21 and 3.22 must behave according to the control inequalities on the right for a potential optimal trajectory to exist.

$$\mu_T \begin{cases} \leq 0 \rightarrow T = T_{\max} \\ = 0 \rightarrow T_{\min} < T < T_{\max} \\ \geq 0 \rightarrow T = T_{\min} \end{cases} \qquad (3.21)$$

$$\mu_\beta \begin{cases} \leq 0 \rightarrow \beta = 2\pi \\ = 0 \rightarrow 0 < \beta < 2\pi \\ \geq 0 \rightarrow \beta = 0 \end{cases} \qquad (3.22)$$

2. Feasibility

Generated trajectories are checked for feasibility by taking the control profile created by DIDO and propagating it through the equations of motion shown in equation 3.3 using the ODE 45 propagator in MATLAB and linear interpolation of the DIDO controls. The propagator trajectory is then superimposed on the optimizer trajectory. A perfect match indicates feasibility.

3. A Word about Scaling

Quantities calculated in the simulations featured here range from the very large (interplanetary distances) to the very small (spacecraft thrust). While employing standard units of measure may be convenient for the reader, such units can be computationally inefficient or even inaccurate. Thus, it becomes necessary to define an alternative method of scaling for fundamental units such as time, distance, and mass. Done properly, this can balance out the calculations in such a way as to ensure well behaved solutions and computational accuracy. These fundamental units are then used to generate derived units such as velocity, acceleration, and thrust. For example, it is convenient to define the unit of mass in terms of the initial spacecraft mass, distance in terms the distance between the Earth and the Sun, and time in terms of a constant force unit,

Mass Unit = 1222 kg = 1 MU

Distance Unit = $1.49598 \times 10^8 km$ = 1 DU

Force Unit = $0.0145 kg \cdot km / \sec^2$ = 1 FU

$$\text{Time Unit} = \sqrt{\frac{MU \times DU}{FU}}$$

$$\text{Velocity Unit} = DU/TU$$

It is occasionally desirable to readjust or rebalance the relationship between all of these units. This is particularly true when the predefined values like rated maximum thrust or spacecraft mass change significantly. Inadequate scaling manifests itself in a number of ways such as a large Hamiltonian, inconsistent propagation, or even through an altogether infeasible solution. The author found it convenient to address this issue by adjusting the value of FU between 0.0145 (for the Hohmann Transfer example) and 0.0148 (for all other examples) until the propagation inconsistencies subsided.

In many of the examples that follow, state variables are plotted in both scaled and unscaled (metric) units for the reader's convenience. If no units are specified, scaled units can be assumed. It should be noted that all the scaled plots that follow display horizontal axes which are numbered in the Time Unit described above. Each Time Unit is approximately equal to 41 days.

THIS PAGE INTENTIONALLY LEFT BLANK

IV. SIMULATING THE ASTEROID SAMPLE RETURN PROBLEM

A. ONE-WAY ORBIT TRANSFERS

Simulation of the sample return mission is an incremental process in which increasingly complex trajectories are modeled, generated, and validated for optimality and feasibility at each step. Once simple trajectories are found to be valid, additional complexities can be encoded into the model that allow the simulation to account for such factors as C3, hyperbolic excess velocity, or eccentric orbits. Once complex one-way trajectories are validated, the code used to generate them is employed to create increasingly complex two way models that ultimately incorporate phasing, as well as rendezvous and capture. Where possible, additional validation is sought by way of comparison with trajectories generated by other researchers.

1. Simple Circular Transfer

A simple Hohmann Transfer was chosen to validate the dynamics and ensure the soundness of the code and scaling. Using a known spacecraft model and a known optimal trajectory with known constraints, an attempt was made to duplicate the results obtained by Lieutenant Scott B. Josslelyn [Ref. 9] and thereby confirm the code's accuracy. The model assumes a 659.3 kilogram spacecraft powered by six NSTAR thrusters with a total maximum rated thrust of 0.55 N and a specific impulse of 3280 seconds. The trajectory is constrained to take the spacecraft from an assumed Earth circular orbit at 1 AU to an assumed Mars circular orbit at 1.52 AU while traveling through no more than 3.14 radians of angular displacement.

Where Jossleyn obtained a final spacecraft mass of 540.3 kilograms, the sample return mission simulator code produced a final mass of 540.7 kilograms. Similarly, where Jossleyn obtained an elapsed time of 253.4 days, the asteroid code generated an elapsed time of 252.8 days. The trajectory shown in Figure 7 is virtually an exact replica of the one obtained by Jossleyn and is similar in appearance to a Hohmann Transfer.

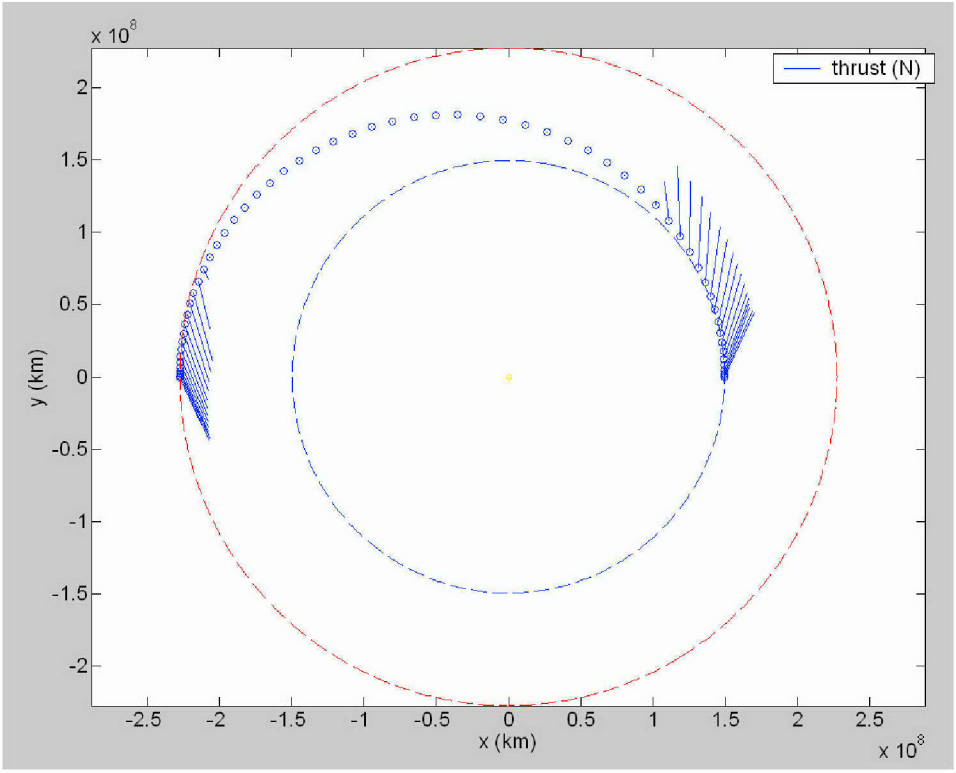

Figure 7. Hohmann Transfer – Trajectory (Unscaled Units)

In addition, the control and state variables plotted in Figure 8 and Figure 9 exhibit smooth, economical, non-erratic behavior with respect to time. Thrust magnitude exhibits a profile characteristic of "bang-bang control" as one would expect in a Hohmann Transfer. These are all traits highly suggestive of a solution that is feasible if not optimal.

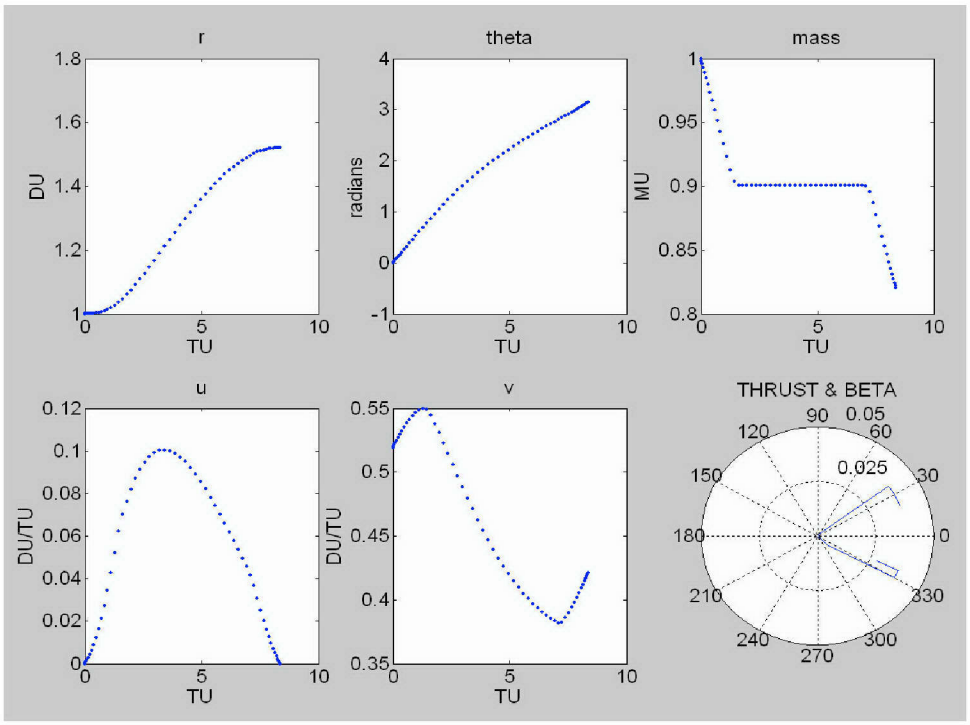

Figure 8. Hohmann Transfer - State and Thrust Angle (Scaled Units)

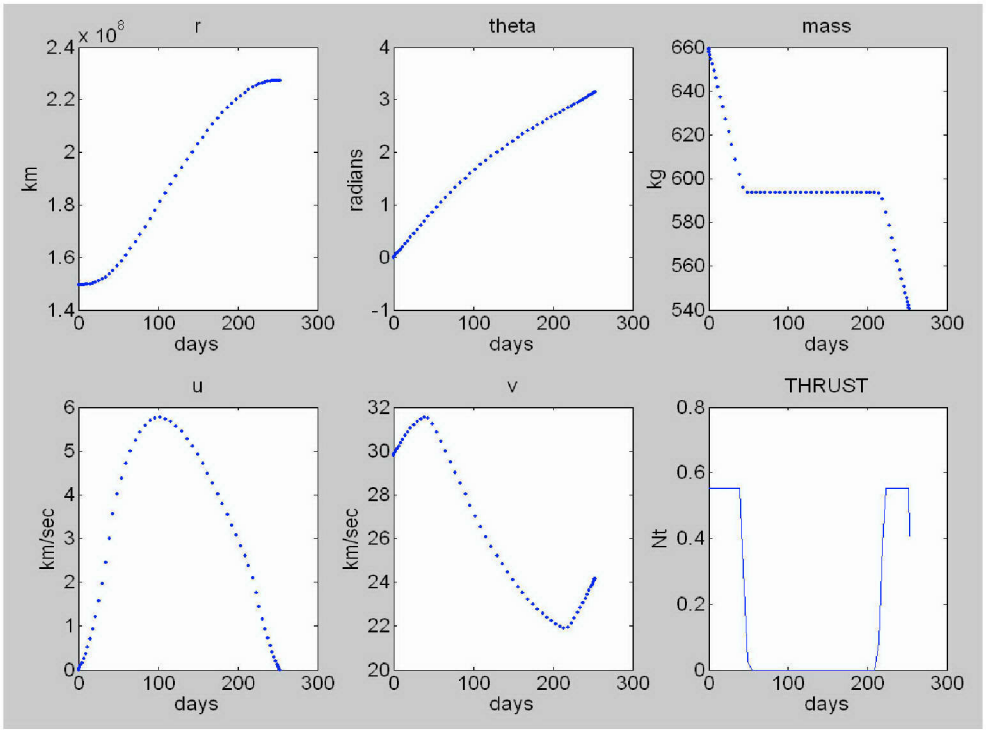

Figure 9. Hohmann Transfer - State and Thrust Magnitude (Unscaled Units)

Optimality is apparent however, in the plots of the Hamiltonian, KKT multipliers, and switching functions with respect to time shown in Figure 10.

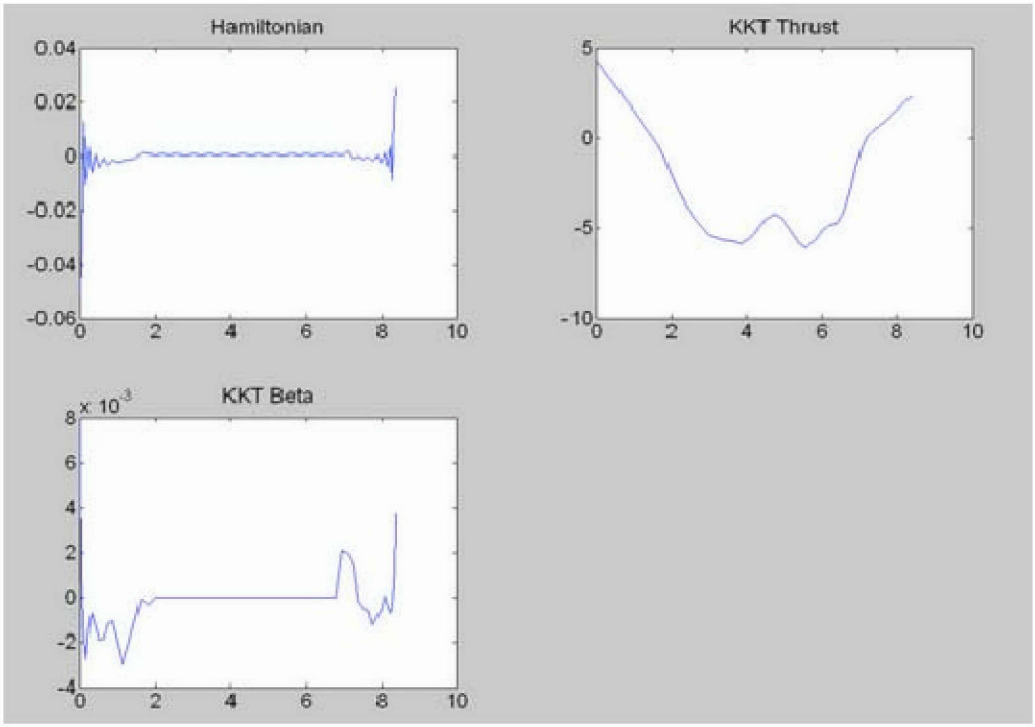

Figure 10. Hohmann Transfer - Hamiltonian and KKT Multipliers (Scaled Units)

That the KKT multiplier for thrust varies somewhat from zero may be due to a problem within DIDO requiring further investigation [Ref. 15]. Non-optimal solutions frequently have KKT thrust values many orders of magnitude higher than the one shown above. This plot suggests that the solution is at least very nearly optimal.

But taken in conjunction with Figure 11, which shows the Complimentarity Condition being met throughout the trajectory, Figure 10 is highly indicative of an optimal solution.

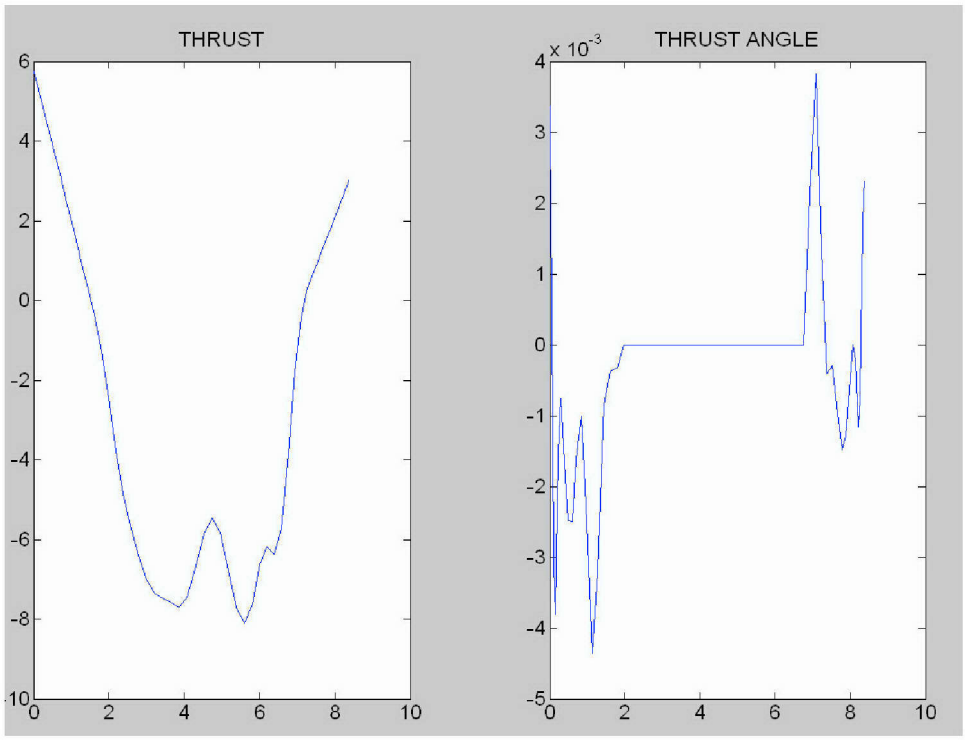

Figure 11. Hohmann Transfer - Switching Functions (Scaled Units)

Finally, feasibility can be inferred based on the appearance of Figure 12; where state trajectory, shown in red, is superimposed on propagated trajectory, shown in blue. The two are virtually indistinguishable.

Thus, the trajectory is in all likelihood optimal and feasible; exhibiting behavior perfectly consistent with the necessary conditions for optimality.

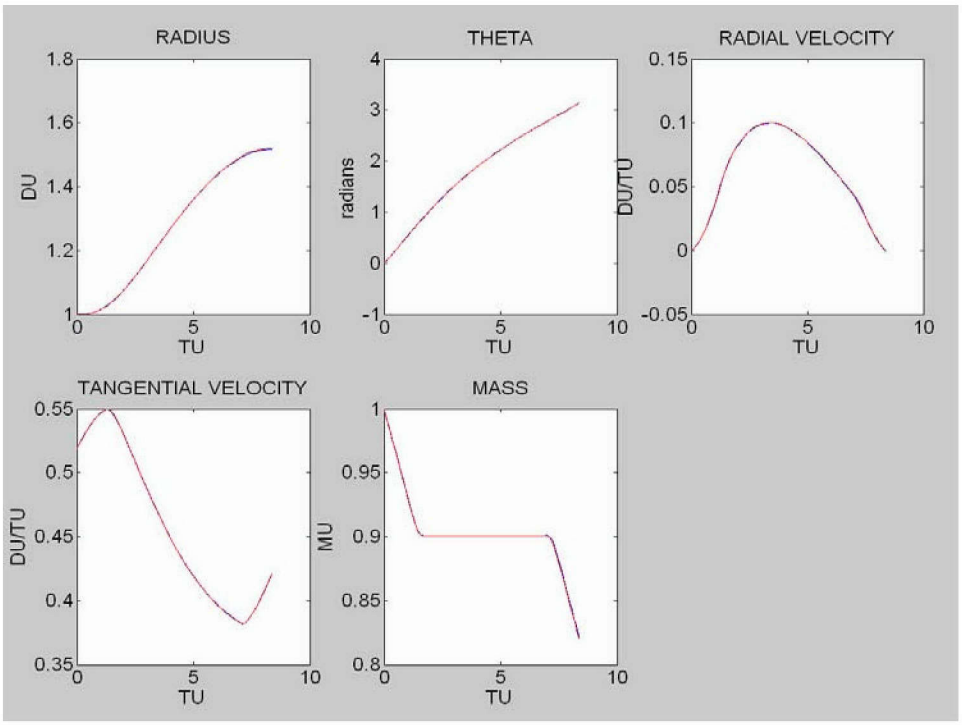

Figure 12. Hohmann Transfer Feasibility Comparison (Scaled Units)

2. Dealing with the Limitations of the Simplified Model

The previous trajectory was generated for a 660 kilogram spacecraft with six thrusters operating at full power. For the purposes of this work, the sample return spacecraft is assumed to be a 1222 kilogram spacecraft with two thrusters operating at less than full power much of the time.

As previously discussed, a real NSTAR ion thruster features a range of mission throttle levels; some of which are shown in Table 1. Each level has a particular thrust setting and a corresponding specific impulse. The choice of what throttle level to employ is dictated not only by trajectory requirements, but also by available power levels. These are in turn a function of available solar flux, battery and solar array condition, electrical loads, and many other factors.

None of this is adequately accounted for in the simulations that follow. The thruster model used here is simplistic and artificial. Specific impulse is fixed throughout the duration of the mission simulation and thrust is allowed to sweep between zero and a designated maximum value irrespective of real-world power

constraints. Moreover, the sweep takes place in a continuous fashion, not in the discrete fashion exhibited by NSTAR. All of this gives rise to the question of how best to account for these artificialities within the limitations of the model.

It is unrealistic to suppose that a real spacecraft will employ maximum thrust or be able to operate at maximum specific impulse at all times due to constraints on available power. It is equally unrealistic to suppose that a real spacecraft will always employ zero or negligible thrust over the course of a voyage since some amount of thrusting is necessary to arrive at the destination. Nevertheless, the inherent limitations of the model force one to choose from between the two extremes.

Thus, it was initially decided to split the difference and assume a maximum thrust about halfway between zero and the maximum thrust value shown at the top of Table 1. The associated specific impulse was obtained by interpolating between the specific impulse values corresponding to throttle levels three and six. While the numbers may not correspond precisely to an actual Mission Throttle Level, they are close enough for the purposes of this analysis.

Subsequent experimentation revealed that increasing the thrust by about one mN to 38.21 mN and changing the specific impulse proportionally to 2867.2 seconds for a given set of mission constraints (including 90 days on the asteroid) resulted in an overall mission fuel expenditure similar to that obtained by the JPL software package known as SEPTOP. This is not to suggest that the results of the simulations discussed in this thesis exhibit anything approaching the accuracy or fidelity of SEPTOP. The highly simplified two body model used here doesn't even begin to compare.

Picking a maximum thrust / specific impulse combination that falls about half way between the two demonstrated performance extremes of the real thruster and that also happens to generate a result roughly consistent with a much higher fidelity simulation might seem crude. But it is also very conservative and should go some way toward compensating for the artificialities mentioned above.

3. Earth to Asteroid Transfer

In addition to using thrust and specific impulse values that fall within NSTAR performance parameters, the Earth to Asteroid transfer improves upon the Hohmann Transfer by modeling the orbit of 1989ML as an ellipse and by providing an allowance for C3 to be imparted to the spacecraft by the booster. For this simulation, C3 was set not to exceed 2.67 $km^2/\sec^2$ so as to emulate the performance of the Delta II launch vehicle [Ref. 16] which can actually launch 1222 kg to a C3 of 2.67 $km^2/\sec^2$. The transfer takes 1.56 years and consumes 67.7 kilograms of Xenon. The resultant optimal trajectory and thrust vector profile is shown below.

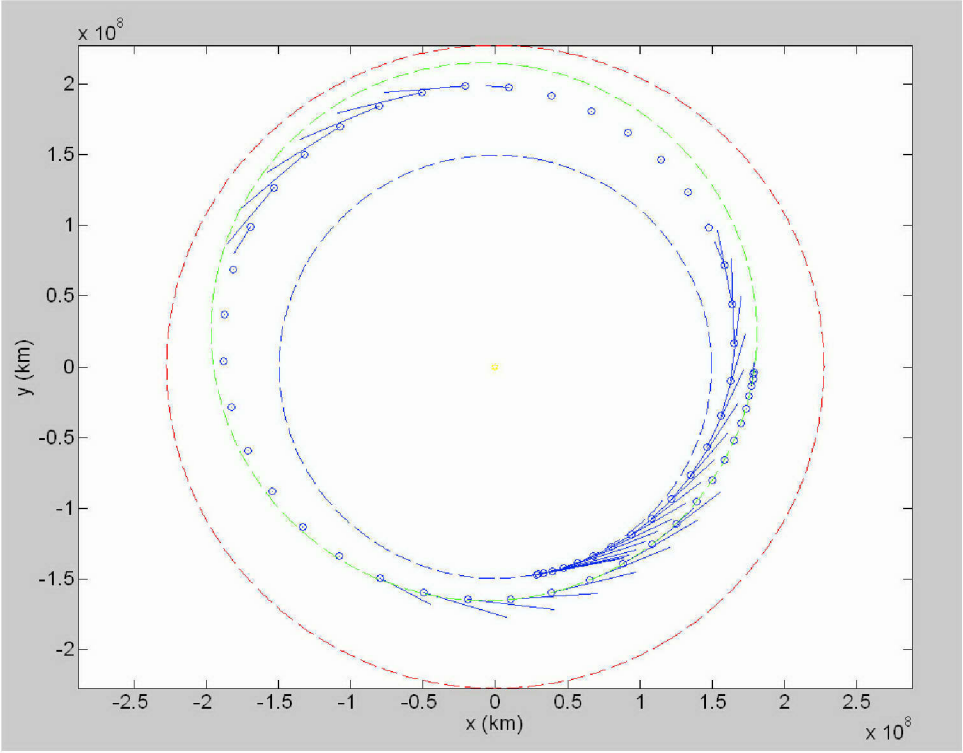

Figure 13. Earth to Asteroid Transfer – Trajectory (Unscaled Units)

It is worth noting that the thrust vectors have a comparatively small radial component. C3 has provided much of the energy needed to accomplish the transfer so the thrusters do not need to contribute that much more. In later

simulations it will be shown that all other things being equal, thrust direction becomes more radial as thrust magnitude is constrained.

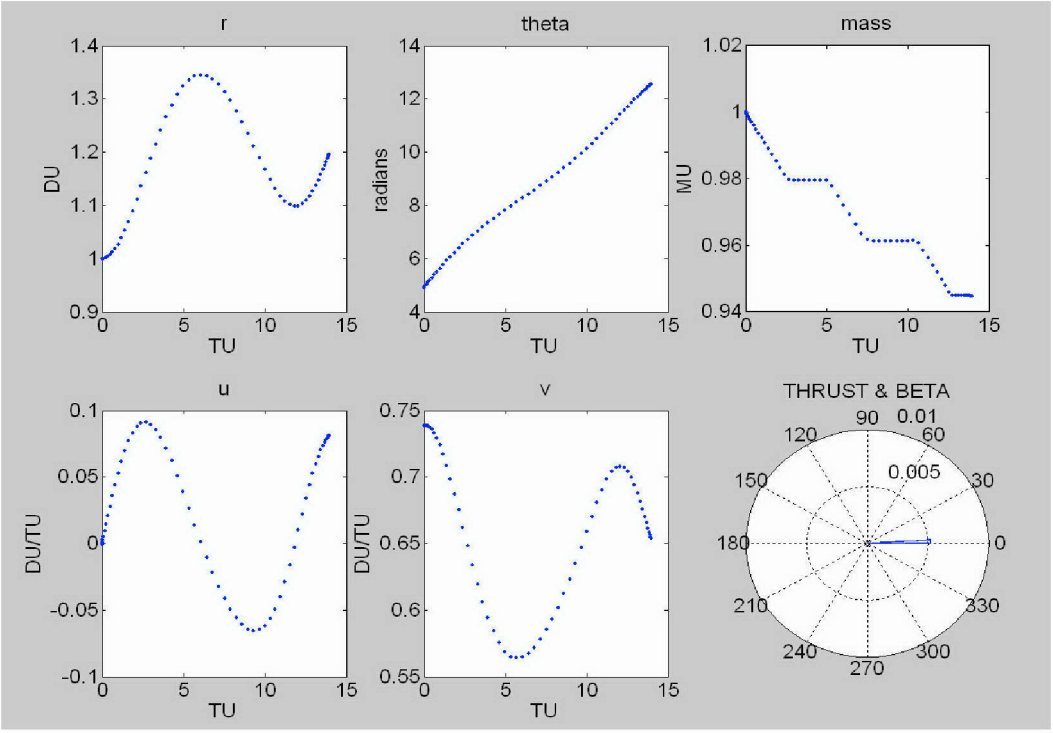

Figure 14. Earth to Asteroid Transfer - State and Thrust Angle (Scaled Units)

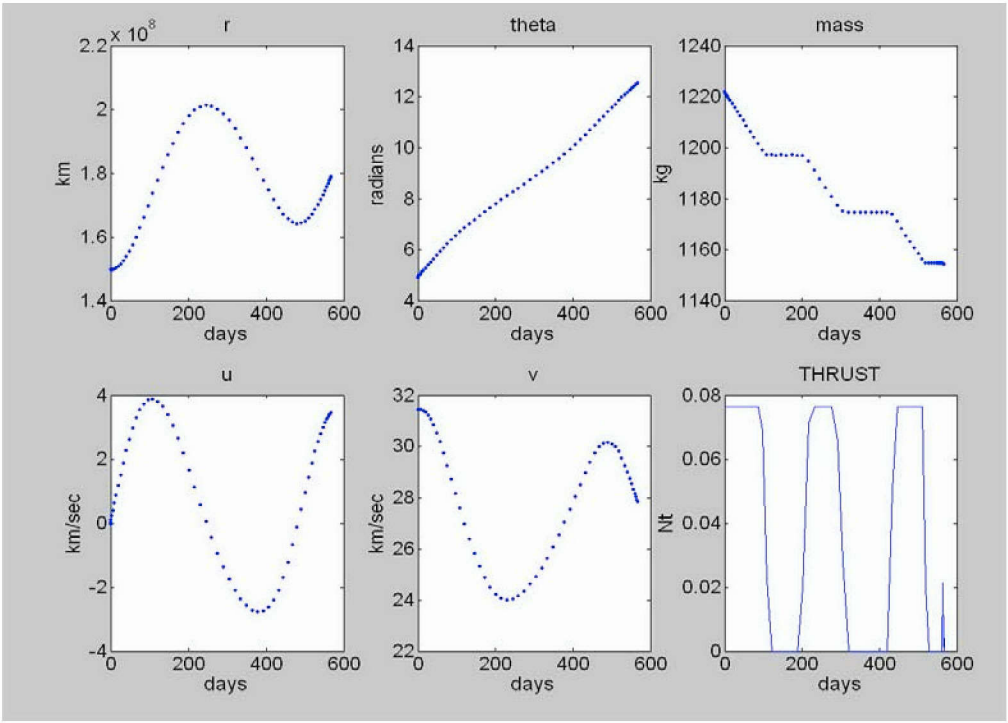

Figure 15. Earth to Asteroid Transfer - State and Thrust Magnitude (Unscaled Units)

Once again, state variables plotted in Figure 14 and Figure 15 appear to exhibit smooth behavior and "bang-bang" control. The Hamiltonian and KKT multipliers are very close to zero. Minor deviations from zero on the part KKT Thrust are due once again to a preexisting problem within DIDO requiring further investigation. A quick glance at Figure 17 verifies that complimentarity has been satisfied and a comparison of the propagated trajectory with the proposed optimal trajectory in Figure 18 shows that the trajectory is feasible.

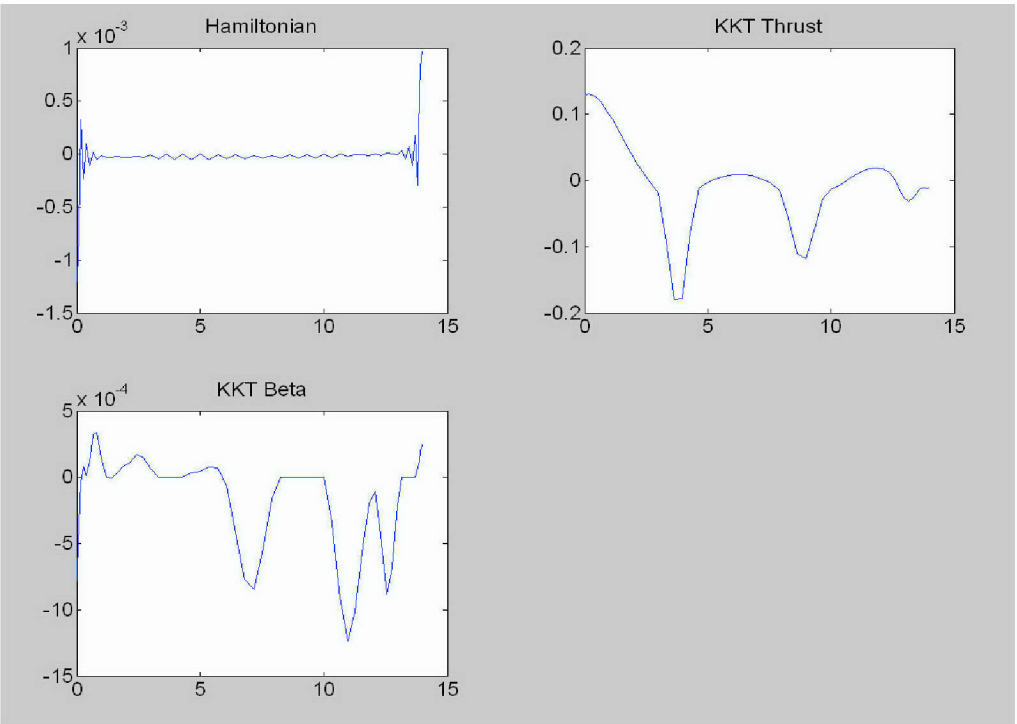

Figure 16. Earth to Asteroid Transfer - Hamiltonian and KKT Multipliers (Scaled Units)

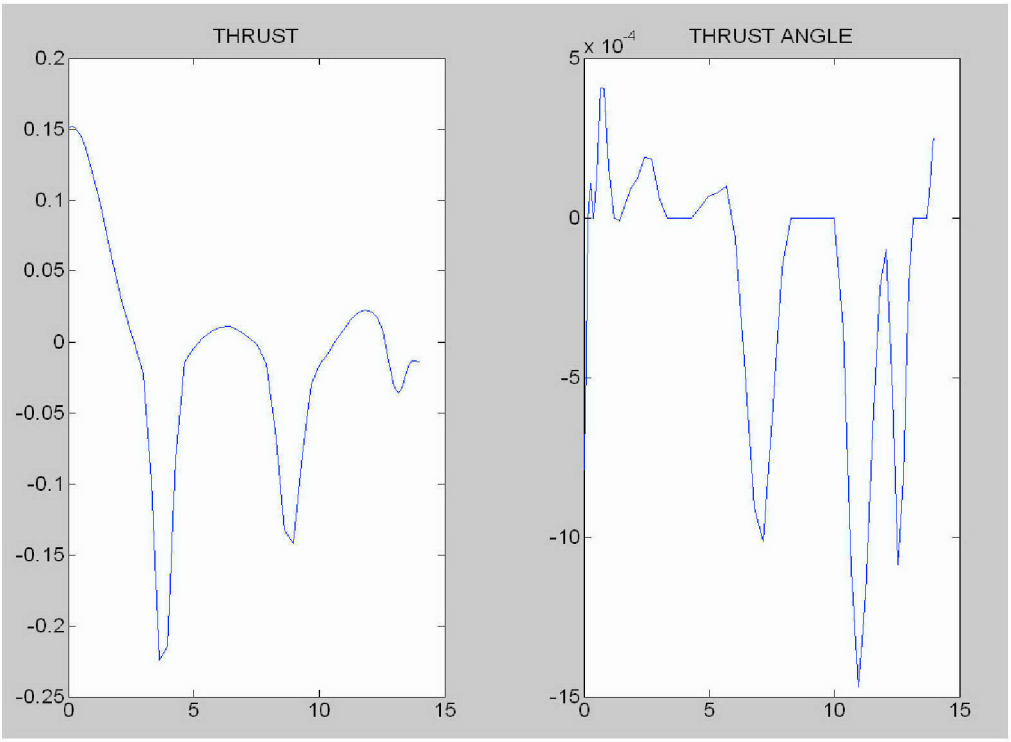

Figure 17. Earth to Asteroid Transfer - Switching Functions (Scaled Units)

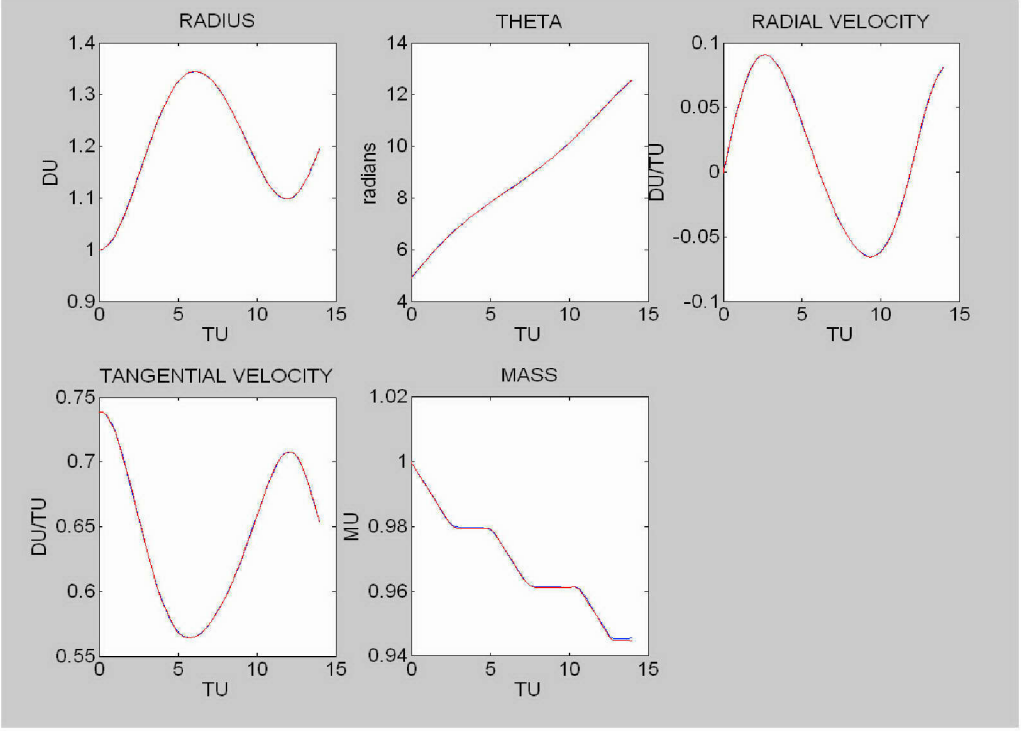

Figure 18. Earth to Asteroid Transfer - Feasibility Comparison (Scaled Units)

4. Asteroid to Earth Transfer

The second half of the asteroid sample return mission shown below entails Earth intercept from elliptical orbit. Hyperbolic excess velocity at Earth is now incorporated into the final event and set not to exceed 3.94 km / sec. The transfer takes 0.84 years to accomplish and consumes 27.35 kilograms of Xenon. Modeling Earth arrival as an intercept as opposed to a rendezvous equates to a considerable savings in fuel since less thrusting is necessary.

As in the previous two trajectories, evidence of optimality is found by virtue of the Minimum Principle and Complimentarity. Results are plotted in Figure 22 and Figure 23. Feasibility is clearly in evidence in Figure 24.

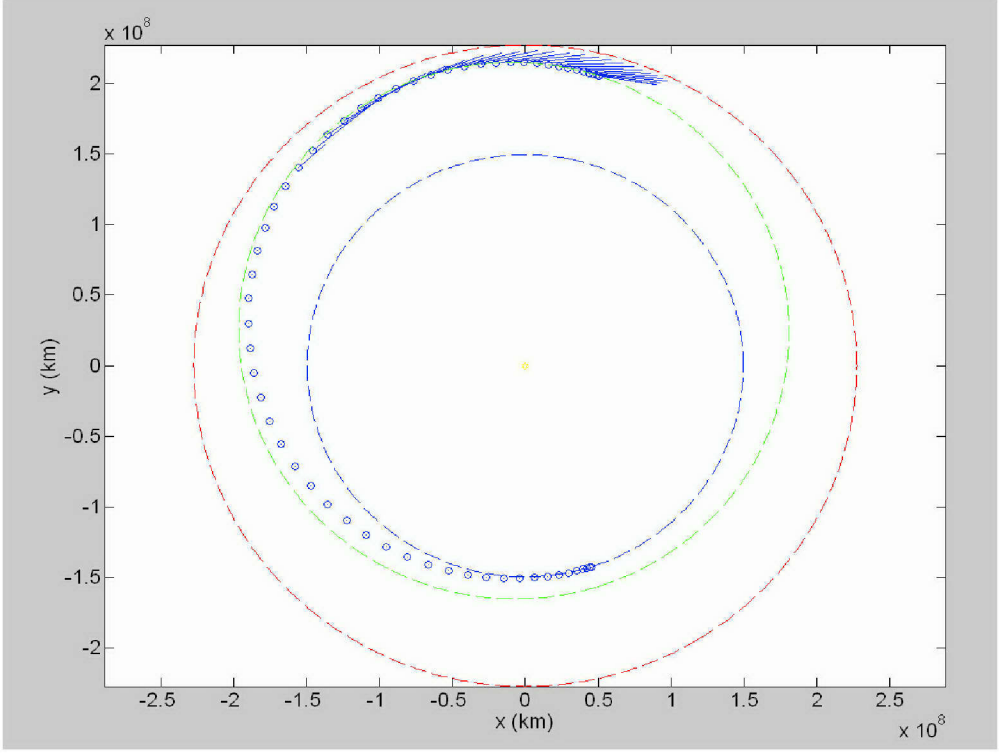

Figure 19. Asteroid to Earth Transfer – Trajectory (Unscaled Units)

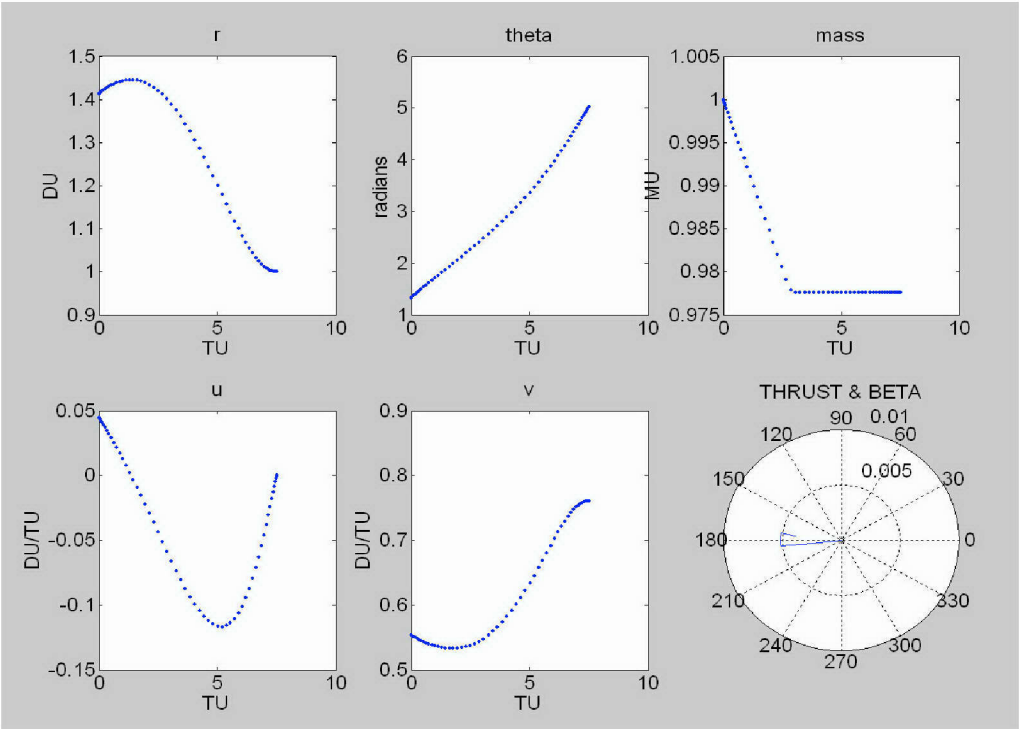

Figure 20. Asteroid to Earth Transfer - State and Thrust Angle (Scaled Units)

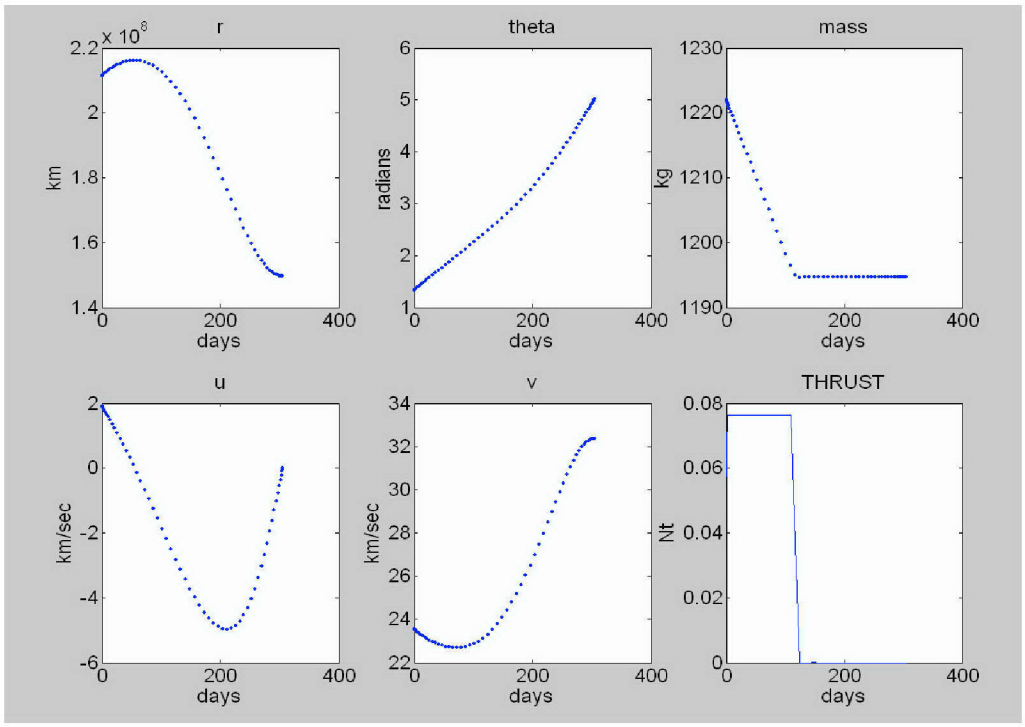

Figure 21. Asteroid to Earth Transfer - State and Thrust Magnitude (Unscaled Units)

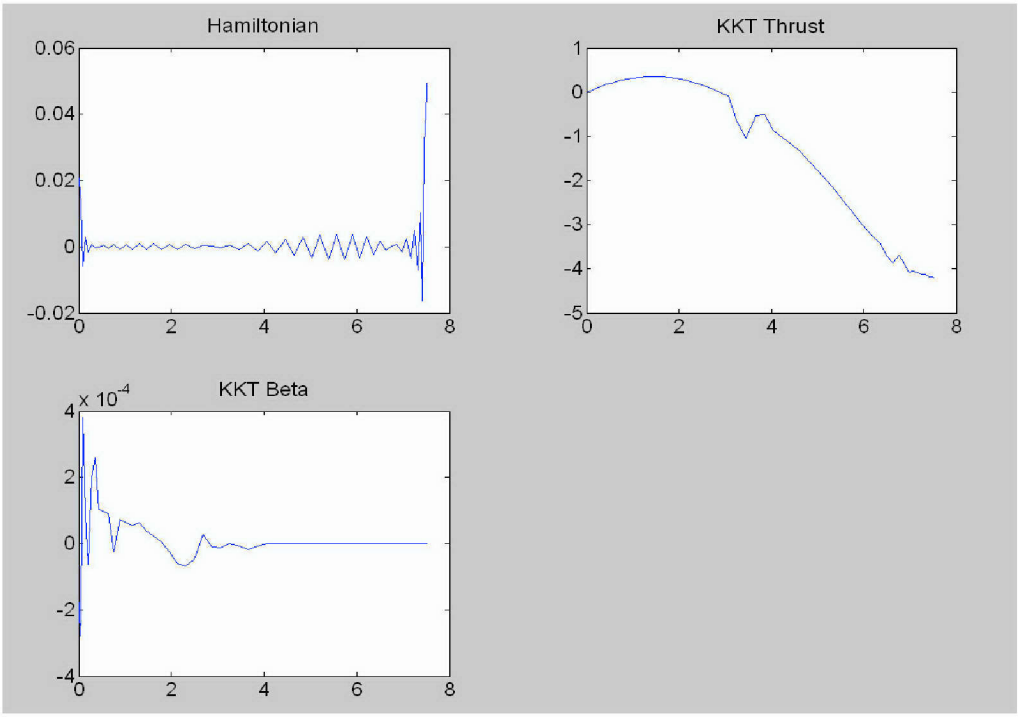

Figure 22. Asteroid to Earth Transfer - Hamiltonian and KKT Multipliers (Scaled Units)

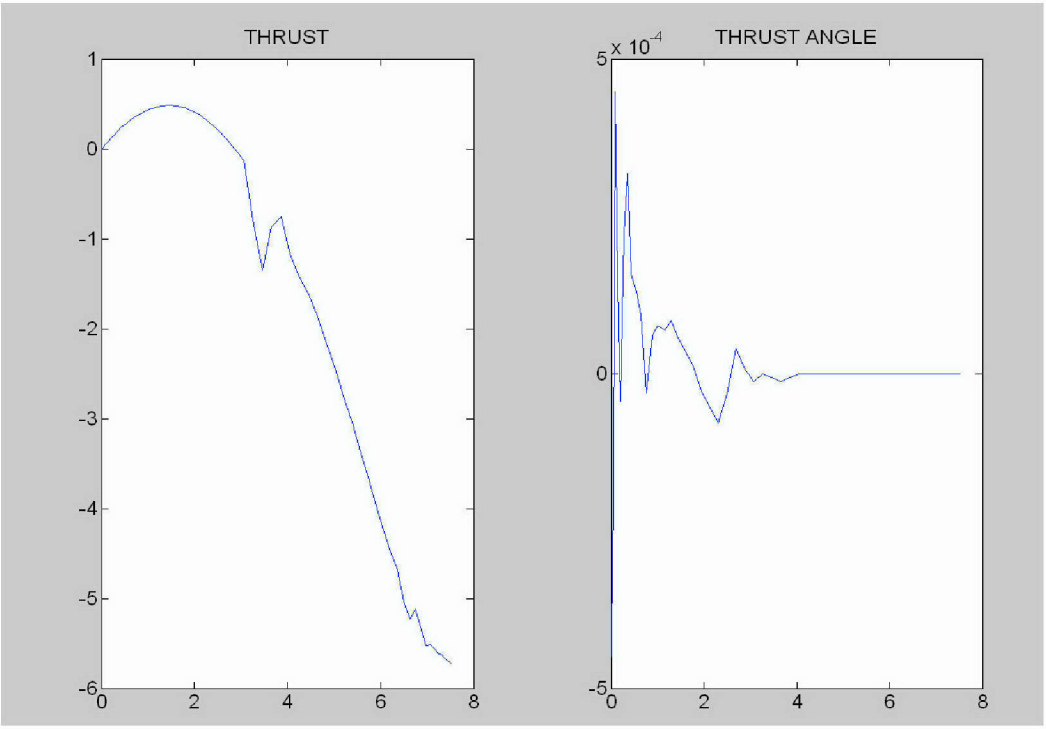

Figure 23. Asteroid to Earth - Transfer Switching Functions (Scaled Units)

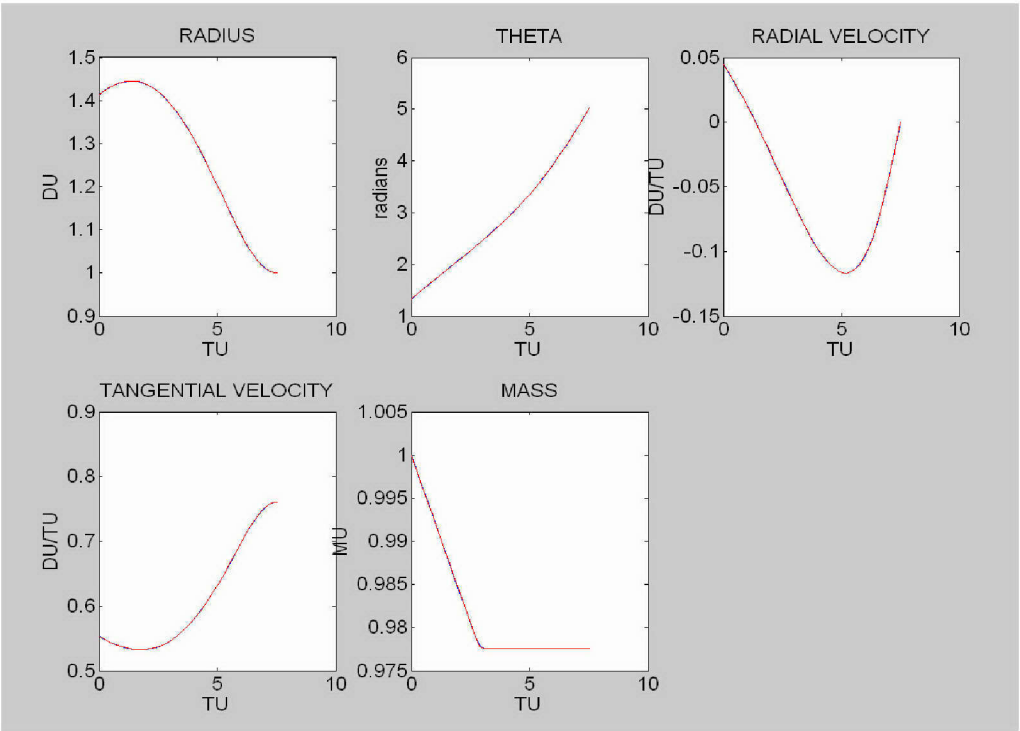

Figure 24. Asteroid to Earth Transfer - Feasibility Comparison (Scaled Units)

B. TWO WAY ORBIT TRANSFERS

1. Unconstrained Surface Time with No Phasing

Having successfully modeled and validated trajectories from Earth to the asteroid and from the asteroid to the Earth, the next logical step is to incorporate everything used thus far into a single round trip simulation. The resulting optimal trajectory allows the spacecraft to stay in the orbit of 1989ML for 355 days. It cannot actually be claimed that the spacecraft has rendezvoused with the asteroid and returned to Earth since phase differences between Earth and 1989ML have yet to be taken into account. That step comes later. For this trajectory, shown in Figure 25, DIDO has elected to use only 2.6 of the allowed 3.94 km / sec in hyperbolic excess velocity. Total fuel consumption is 93 kilograms and total mission time is 3.98 years. It is also worth noting that DIDO has elected to place the points of launch and return to Earth near asteroid perihelion while placing the asteroid arrival and departure points in the vicinity of asteroid aphelion. There is almost a symmetry in the trajectory and thrust profile that mirrors the symmetry of the 1989ML orbit itself. The outbound portion of the trajectory is denoted in blue. The inbound or return trajectory is denoted in red.

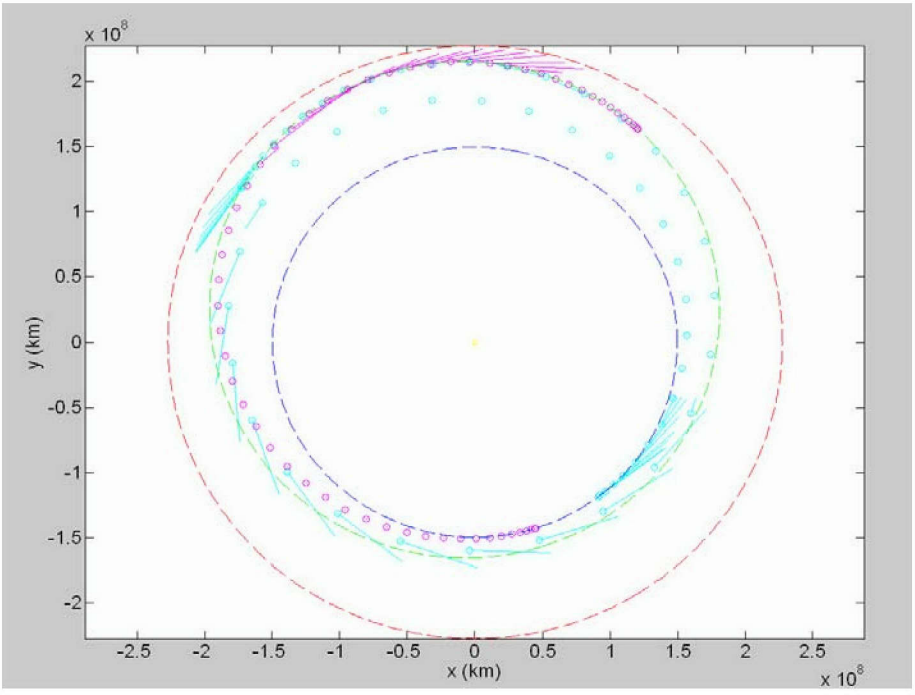

Figure 25. Unconstrained Surface Time with no Phasing - Trajectory (Unscaled Units)

The discontinuities appearing in the state variable profiles of Figure 26 and Figure 27 mark the point at which trajectory optimization stopped and then started up again. These were described earlier as the left and right interior events between which the spacecraft is said to be co-orbiting with 1989ML such that no thrusting occurs and no trajectory optimization is necessary.

Figures 28 and Figure 29 show the propagated trajectory superimposed on the optimal trajectory for the outbound and inbound transfers respectively. Separating the two halves of the trajectory makes it easier to see that the trajectories appear to be virtually identical. This once again serves to verify feasibility.

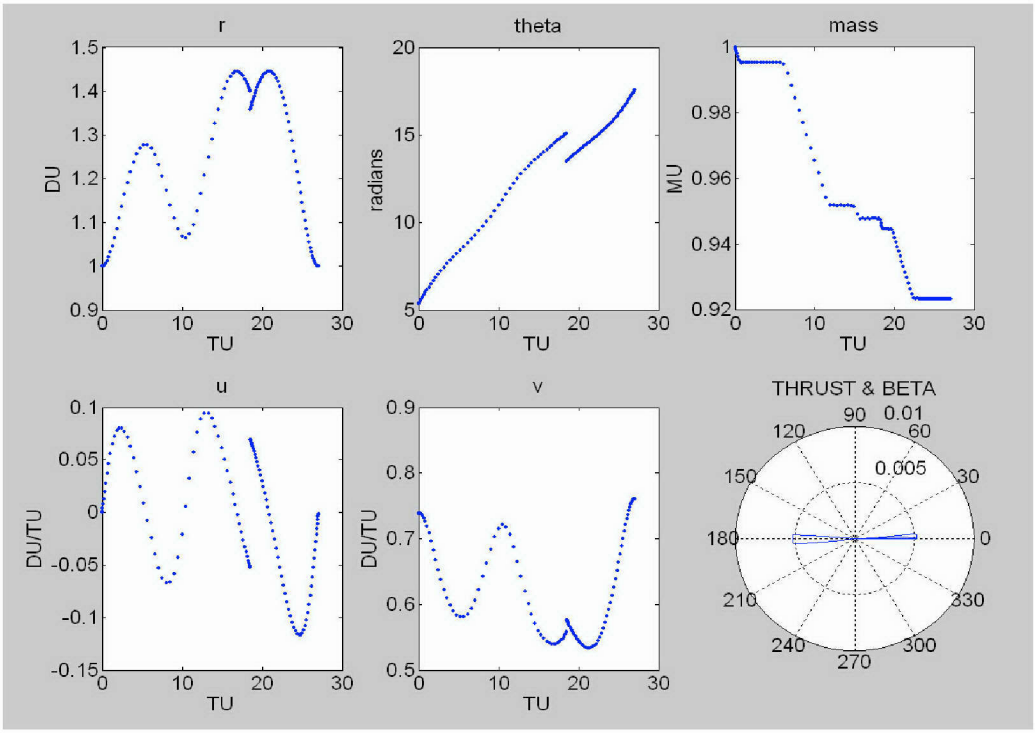

Figure 26. Unconstrained Surface Time with no Phasing - State and Thrust Direction (Scaled Units)

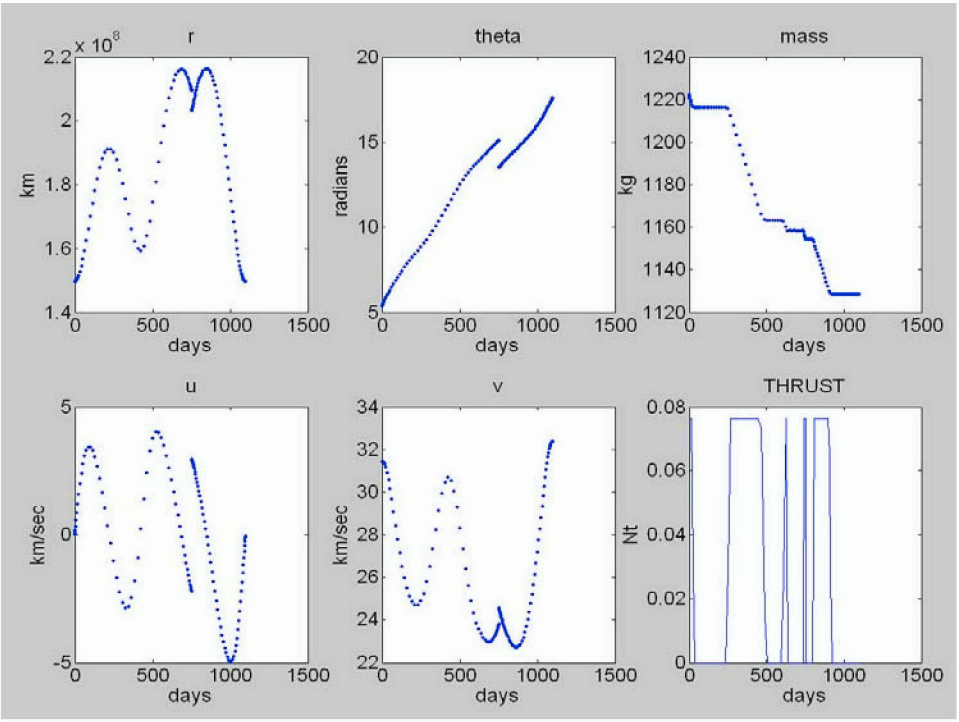

Figure 27. Unconstrained Surface Time with no Phasing - State and Thrust Magnitude (Unscaled Units)

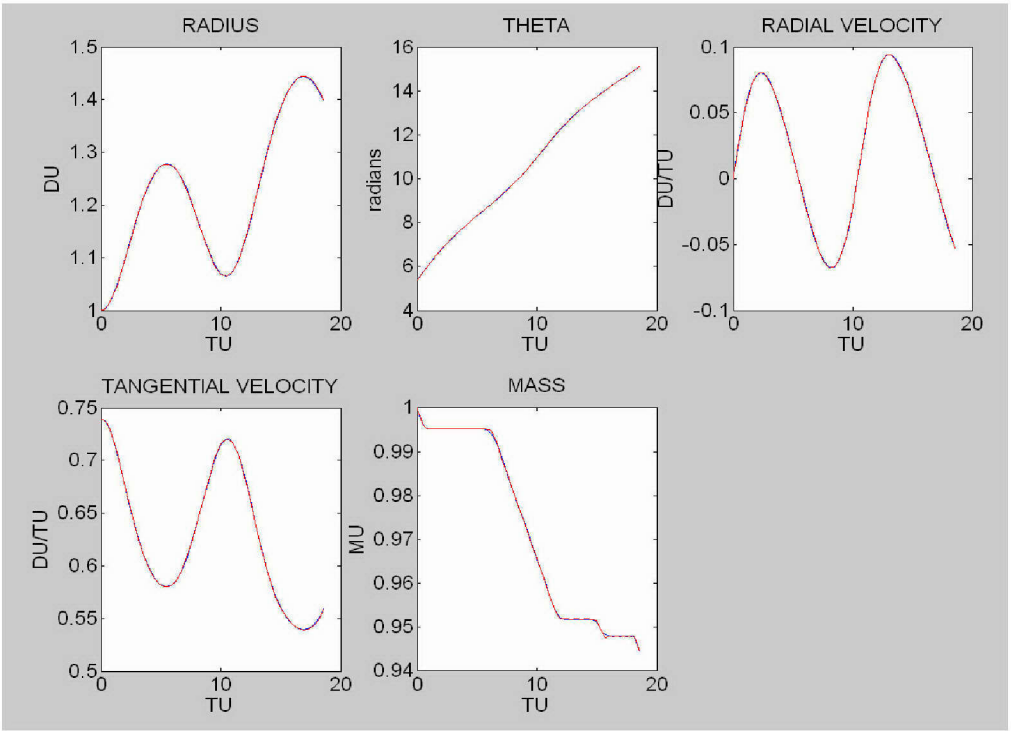

Figure 28. Unconstrained Surface Time Outbound - Feasibility Comparison (Scaled Units)

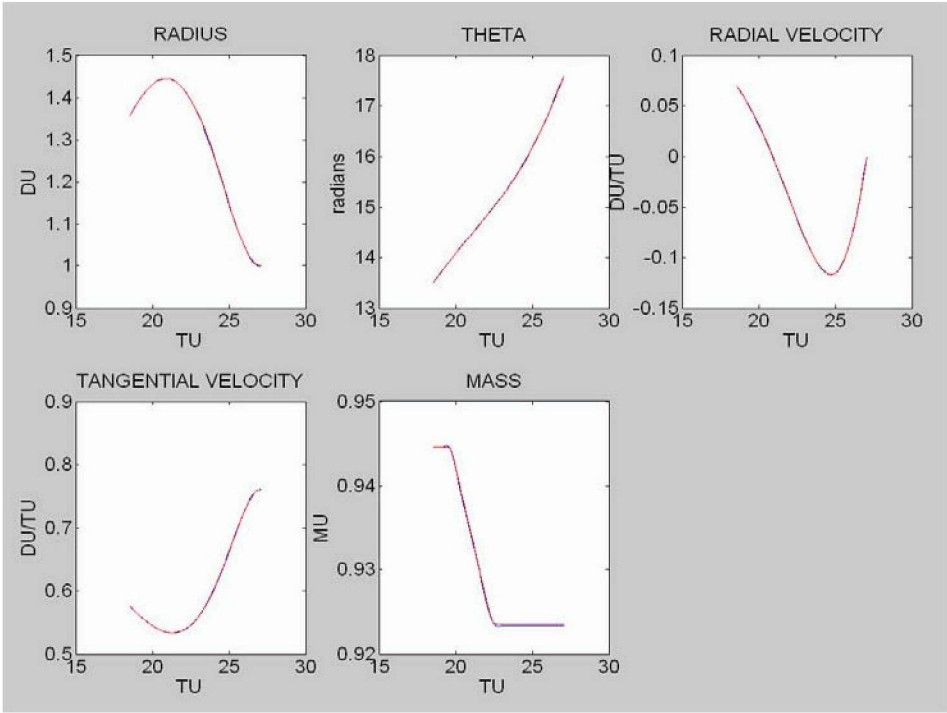

Figure 29. Unconstrained Surface Time Inbound - Feasibility Comparison (Scaled Units)

2. Unconstrained Surface Time with Phasing

The next step involves using mean anomaly as discussed previously to impose the condition that the spacecraft return to Earth orbit at the point where Earth is actually located at the end of the mission. The first thing to notice is that fuel consumption increases dramatically to 156 kilograms of Xenon. Unlike the previous case in which phasing was not accounted for; this time the spacecraft can actually be said to have landed on 1989ML and returned to Earth. However the phasing constraint permits a stay of only 28 days. A longer stay would require more fuel and be less efficient. As in the previous example, discontinuities in the state variable plots show that no optimization is taking place while the spacecraft is on the asteroid surface. Once again, the outbound and inbound trajectory propagations confirm the feasibility of the solution as shown in Figure 33 and Figure 34.

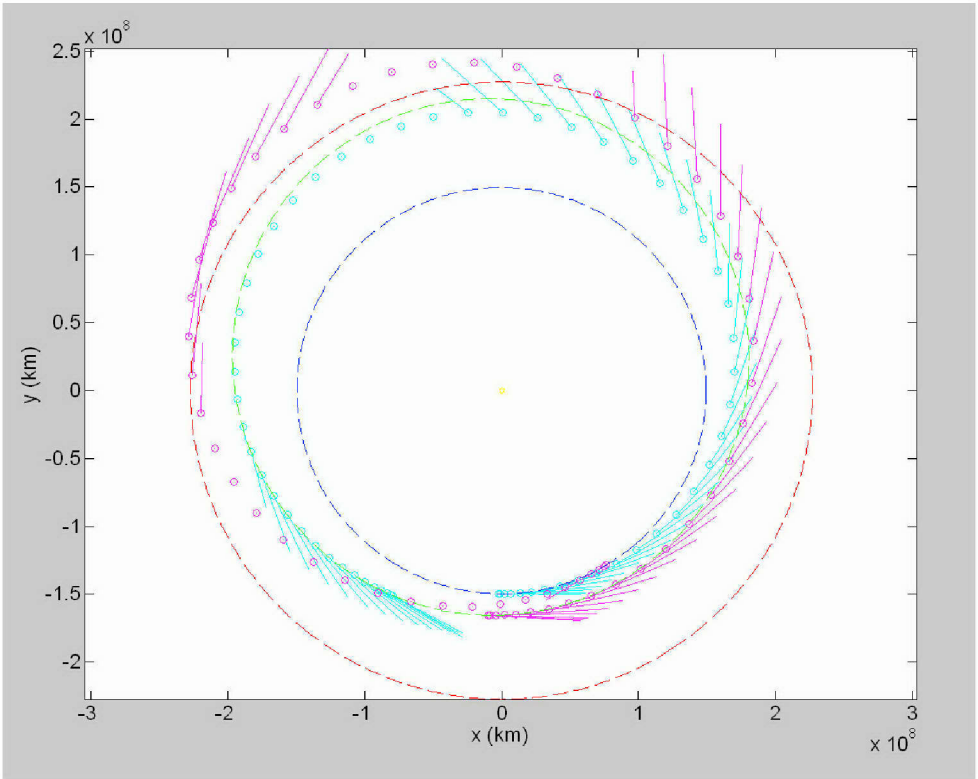

Figure 30. Phasing – Trajectory (Unscaled Units)

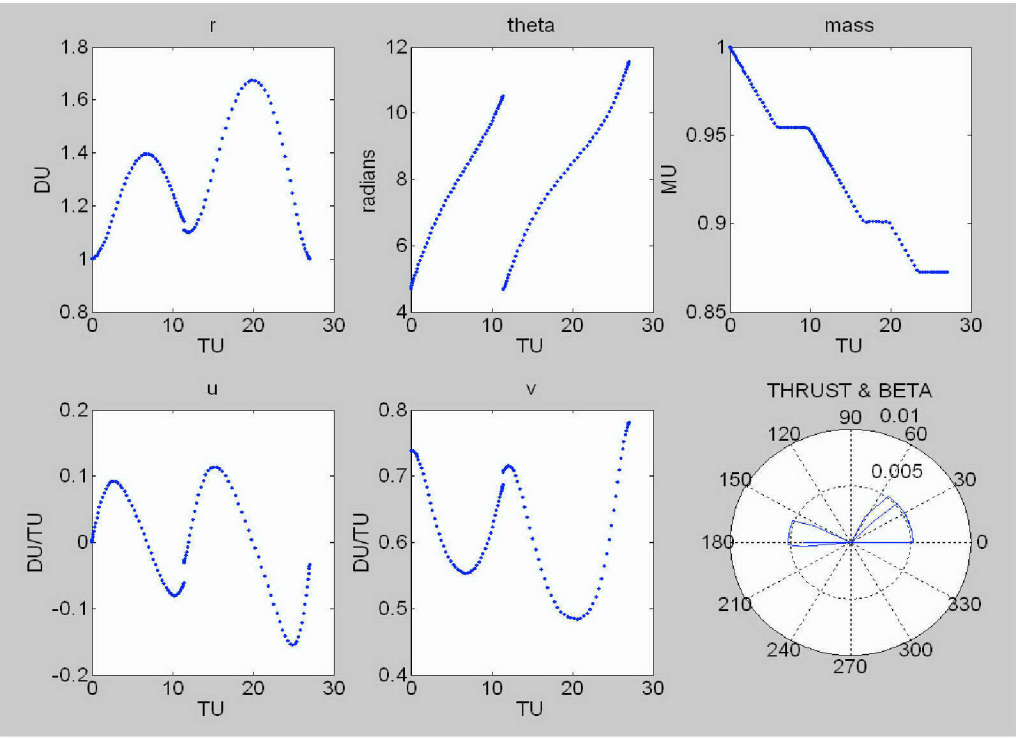

Figure 31. Phasing - State and Thrust Direction (Scaled Units)

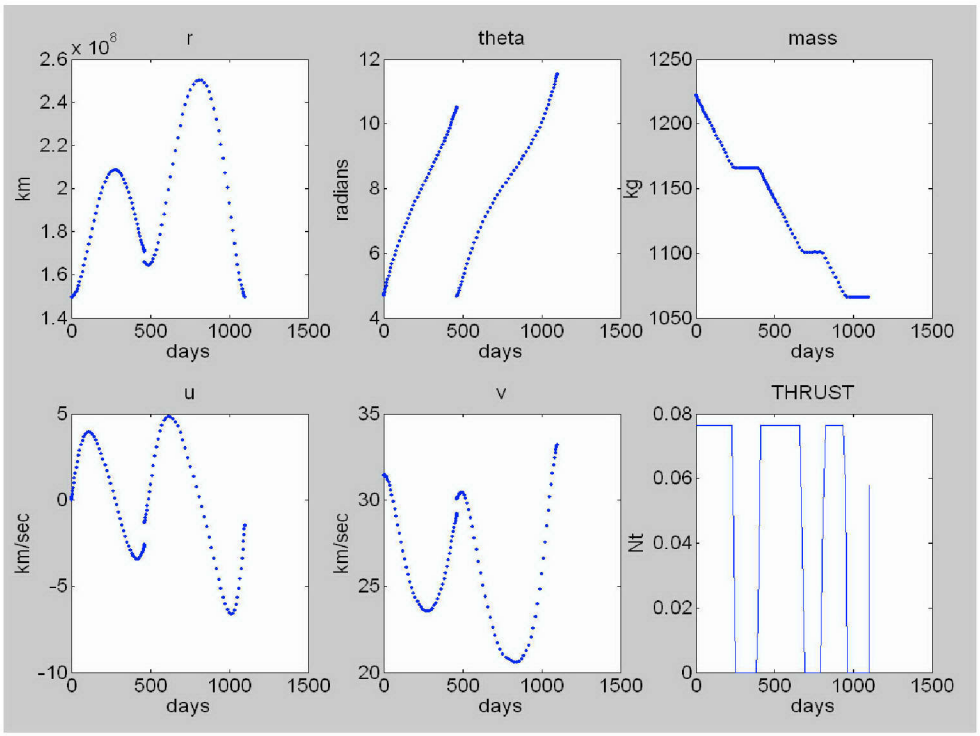

Figure 32. Phasing - State and Thrust Magnitude (Unscaled Units)

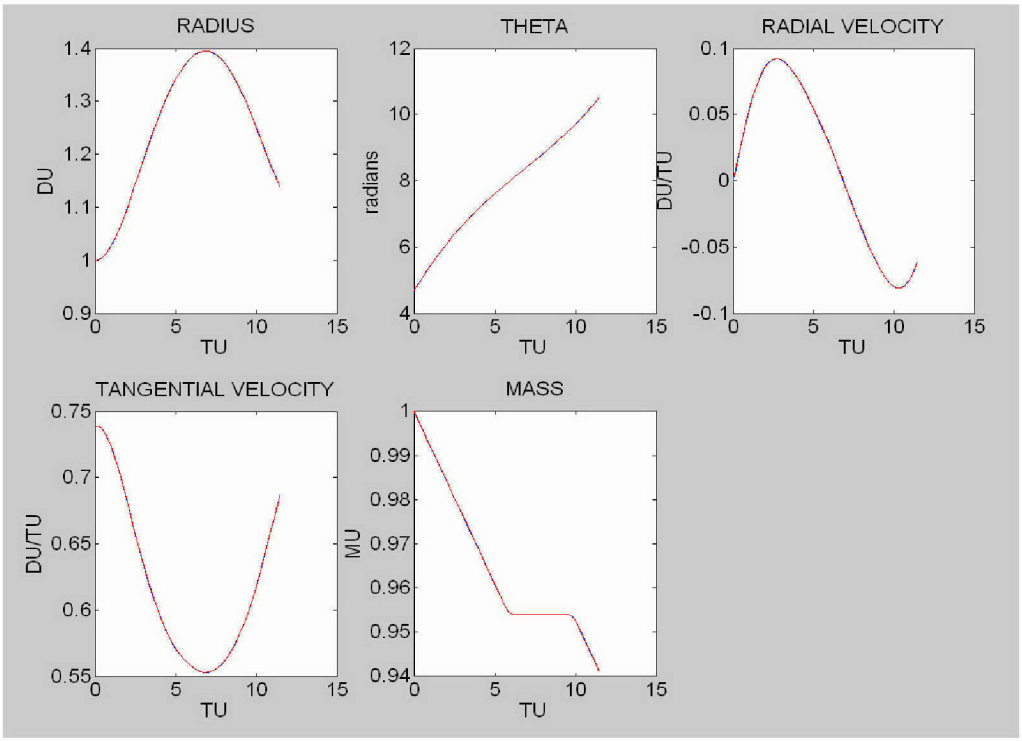

Figure 33. Phasing - Outbound Feasibility Comparison (Scaled Units)

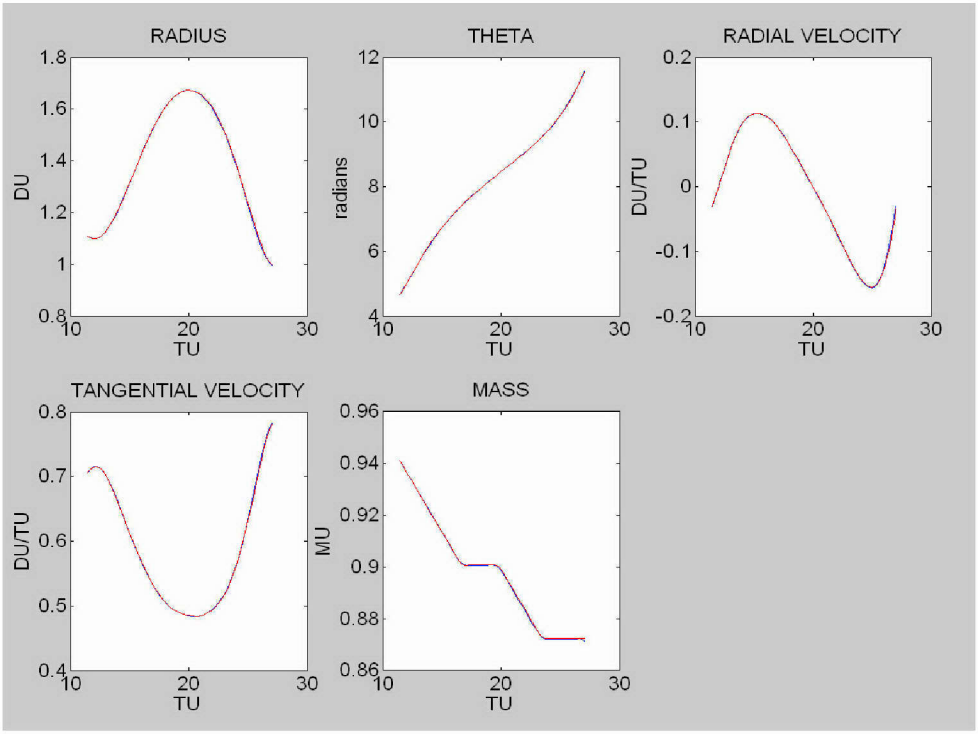

Figure 34. Phasing - Inbound Feasibility Comparison (Scaled Units)

3. Constrained Surface Time with Phasing

The final step in modeling the full sample return is to enable the mission to be simulated with asteroid surface time constrained to a specific value or range of values. As discussed earlier, this is done by making use of the left and right mean anomalies calculated for each of the two interior events.

Figure 35 shows this comprehensive model trajectory for a 90 day asteroid visit. Total mission time is 3.17 years. C3 is 2.67 $km^2/\sec^2$ and hyperbolic excess upon Earth return is 3.2 km / sec. Total mission fuel consumption is 180.13 kilograms of Xenon.

Figure 36 and Figure 37 show the associated scaled and unscaled state and control variables while Figure 38 and Figure 39 illustrate that the trajectory is in fact feasible.

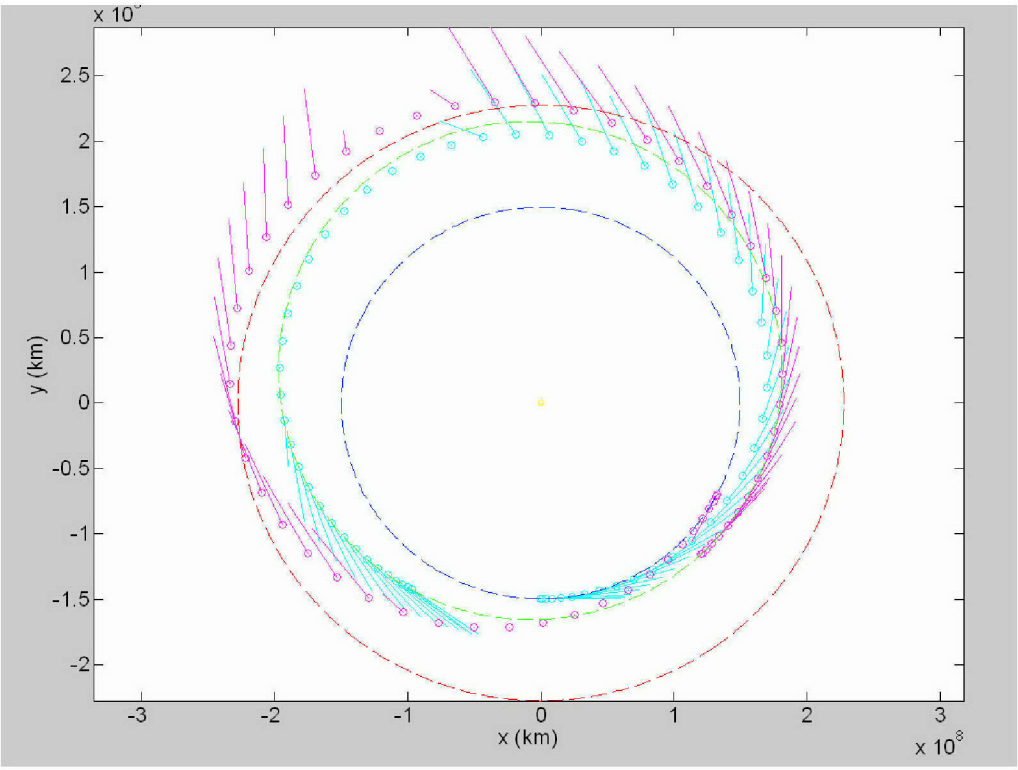

Figure 35. Comprehensive Model – Trajectory (Unscaled Units)

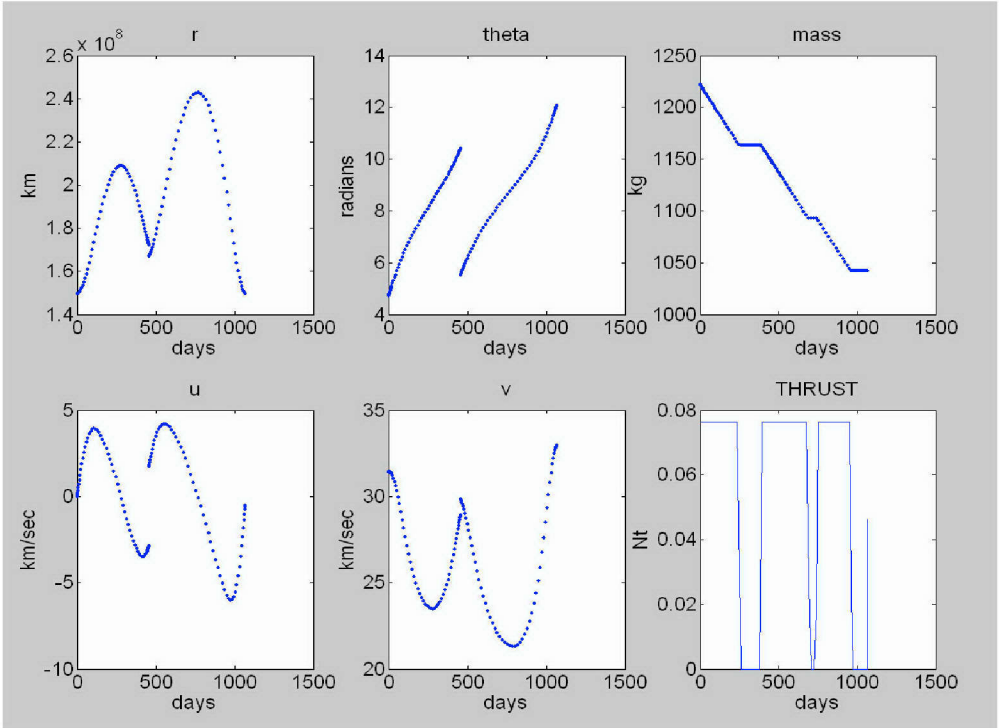

Figure 36. Comprehensive Model - State and Thrust Magnitude (Unscaled Units)

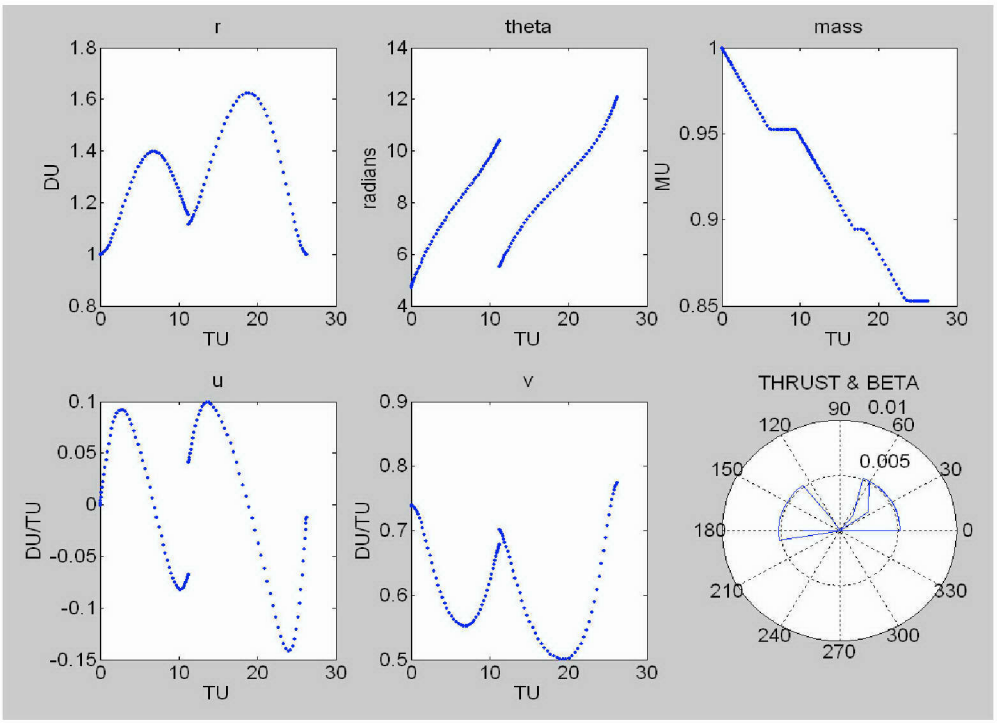

Figure 37. Comprehensive Model - State and Thrust Direction (Scaled Units)

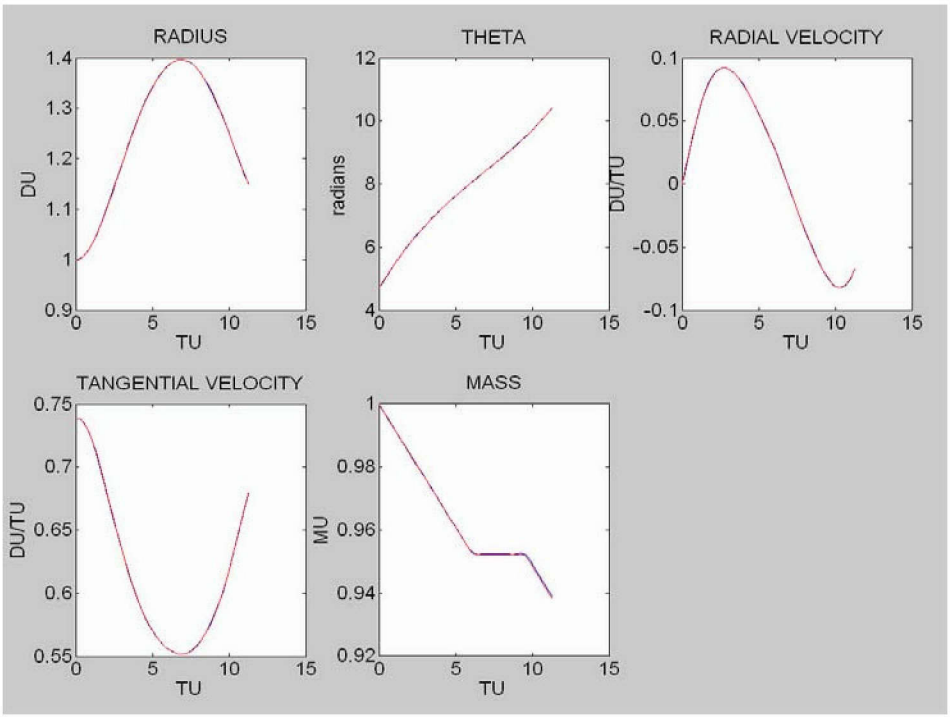

Figure 38. Comprehensive Model Outbound - Feasibility Comparison (Scaled Units)

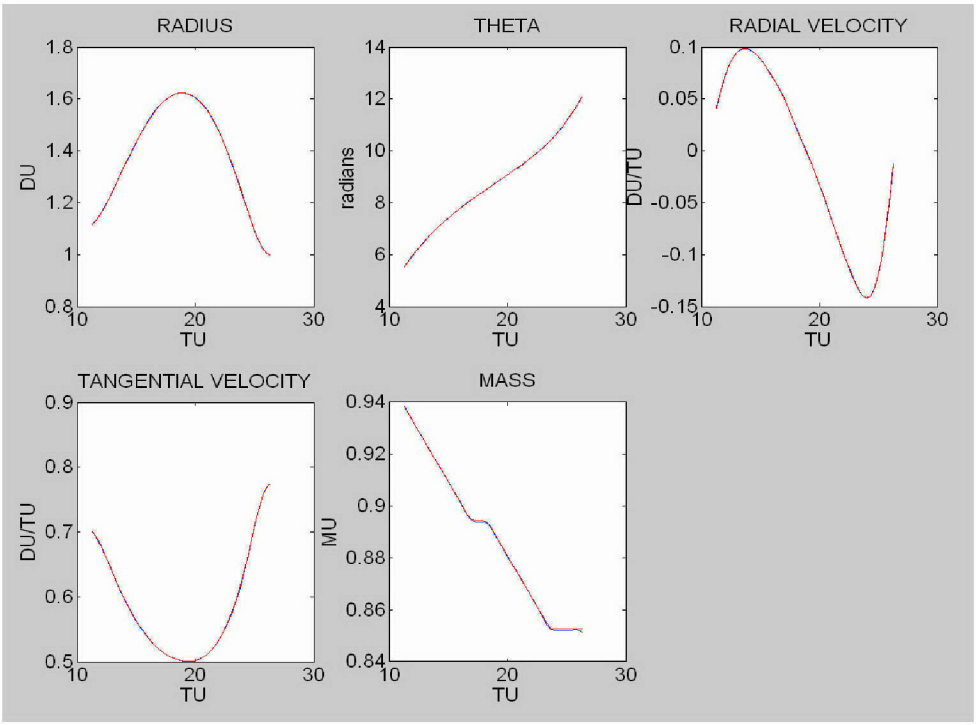

Figure 39. Comprehensive Model Inbound - Feasibility Comparison (Scaled Units)

4. Comparison with SEPTOP Result

Comparing the results of a high fidelity, n-body, three dimensional model like SEPTOP with the results of the highly simplified 2-body, two dimensional model can be misleading. Nevertheless, there are interesting similarities between the SEPTOP result shown in Figure 40 and the Comprehensive Model result shown in Figure 35. Asteroid surface time is the same. The arrival and departure points between orbits occur at roughly the same positions. Total flight time is roughly the same. C3 is the same as are wet mass and propellant mass. There are lesser similarities in hyperbolic excess velocity and outbound thrust profile.

Fixed values for maximum thrust and associated specific impulse were extrapolated from Table 1 in such a way as to result in a fuel expenditure consistent with Figure 40 while keeping near the middle of the thrust range. Nevertheless, the fact that all the other similarities mentioned above fell in to place at the same time suggests that even the highly simplified model might be

sophisticated enough to prove useful in formulating fast rough estimates of how changes in asteroid surface time can affect required fuel load.

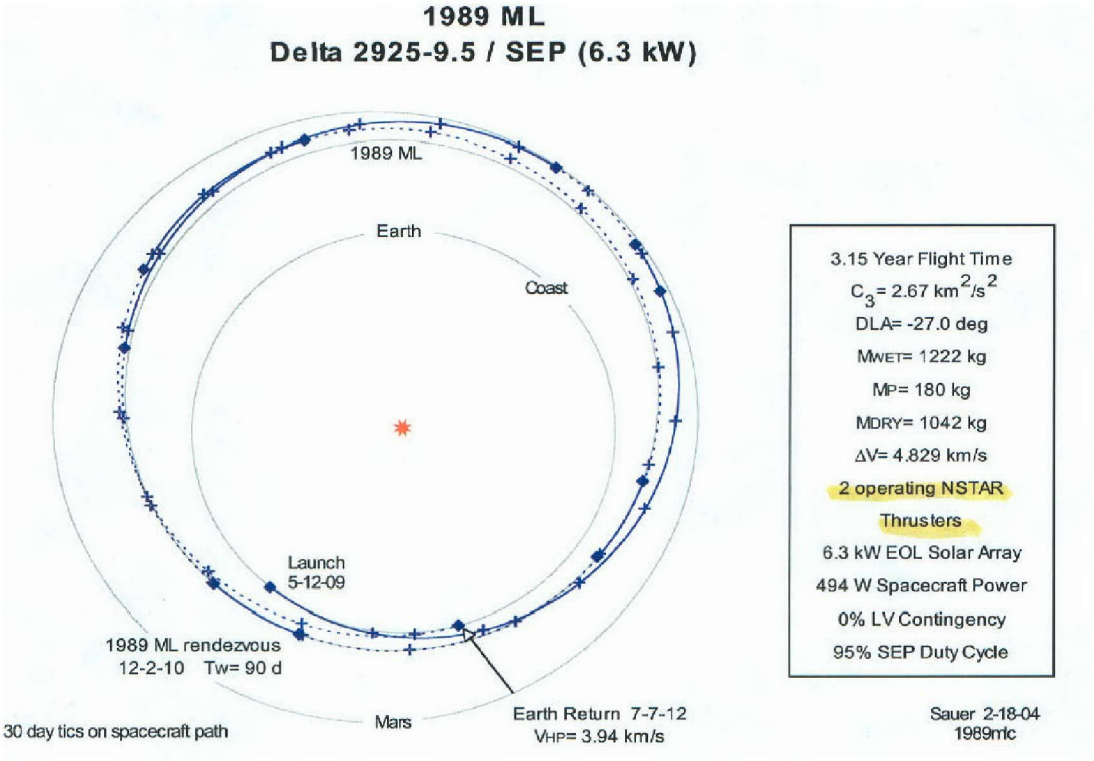

Figure 40. SEPTOP Trajectory Diagram (Courtesy of JPL)

C. VARYING THE SURFACE TIME AND EFFECT ON FUEL

A maximum thrust of 35.14 mN and a corresponding interpolated specific impulse of 2821.6 seconds was used to generate the top line in Figure 41. The combination constitutes the lowest throttle level that can be employed with this code to yield feasible results over a significant range of asteroid surface times. Similarly, a maximum thrust of 75.34 mN and a corresponding specific impulse of 3035 seconds (Throttle Level 12 from Table 1) was used to generate the bottom line. The "R squared" value denotes the square of the correlation coefficient between the points plotted and the equation of the straight line drawn through them. Perfect correlation in the linear regression of the top two lines would result in a value of one. This won't be true of the bottom line since the slope is very close to zero. But the correlation is evident at a glance.

Thus, the top and bottom lines, derived by testing the demonstrated operating extrema of the DS 1 NSTAR thruster as described in Table 1, constitute best and worst case relationships. At worst, staying an extra day on 1989ML will cost no more than 0.64 kilograms of fuel. At best, it will cost next to nothing. Most likely, it will cost something in between. The middle line is derived from the maximum thrust / specific impulse combination that matched the SEPTOP results. It suggests that additional time spent on the asteroid can be purchased at a cost of 0.5 kilograms of fuel per day.

Attempts to extend these lines further to the right resulted in infeasibilities. This suggests that at some point, no amount of fuel will get the spacecraft back to Earth on time. However, High specific impulse and high thrust certainly increases one's options and flexibility.

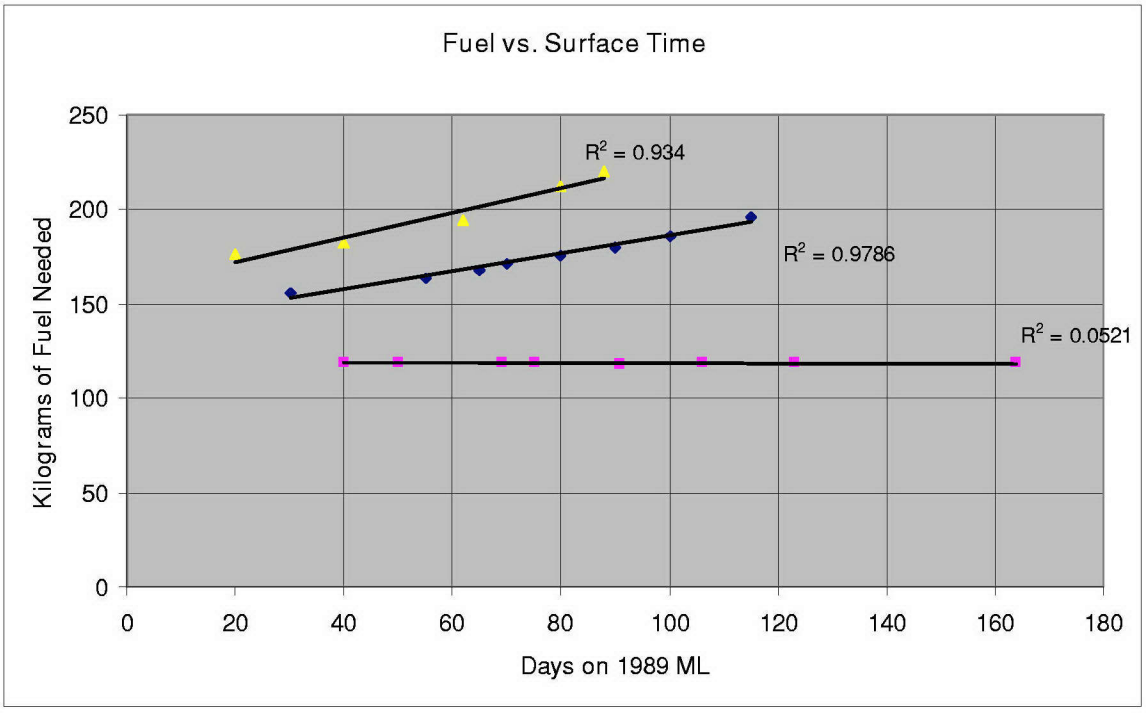

Figure 41. Fuel Versus Stay Time

D. A TENDENCY TOWARD RADIAL THRUSTING

In the course of research, it was frequently observed that optimal thrust angle trajectories for spacecraft that needed to thrust a great deal in order to complete a transfer tended to become more radial as the spacecraft approached

aphelion. At first, this was attributed to a plotting error since radial thrusting does not strike this author as being particularly efficient much less optimal.

The phenomena can be observed in the following trajectory plots. The same code was used to generate Figures 42, 43, and 44. They show comprehensive model trajectories for asteroid sample return missions of 106, 110, and 100 day surface times respectively. The only difference between them is that maximum available thrust and specific impulse is progressively constrained from Figure 42 onward. Each trajectory was found to be both optimal and feasible.

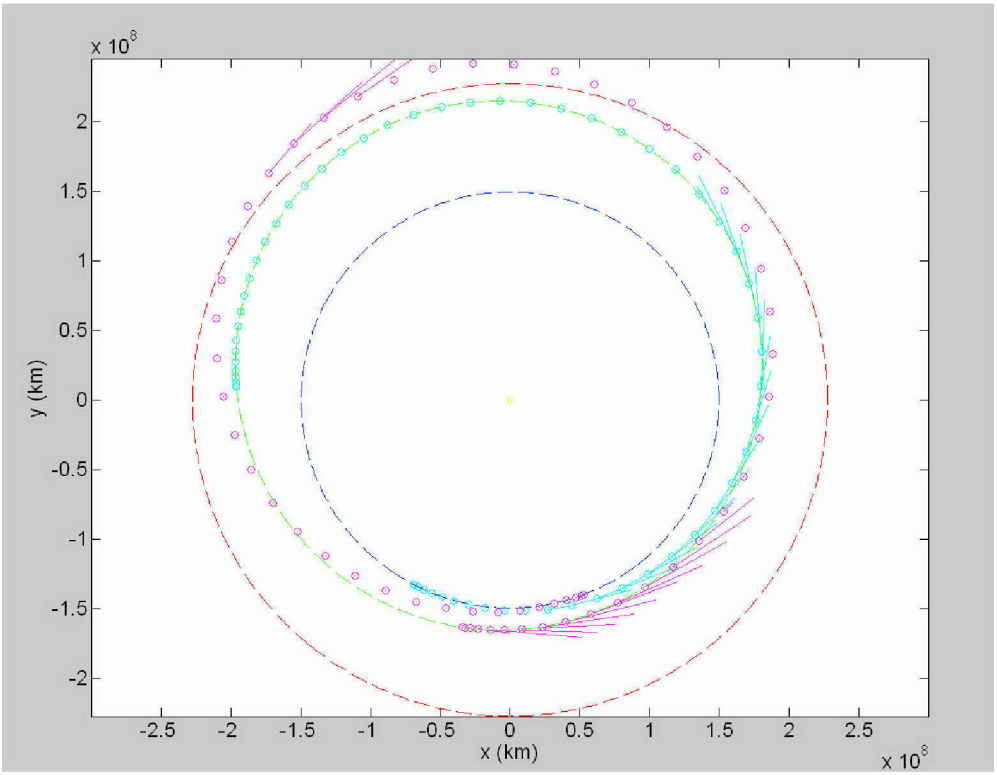

Figure 42. 75.3 N at 3035 sec (106 day surface time)

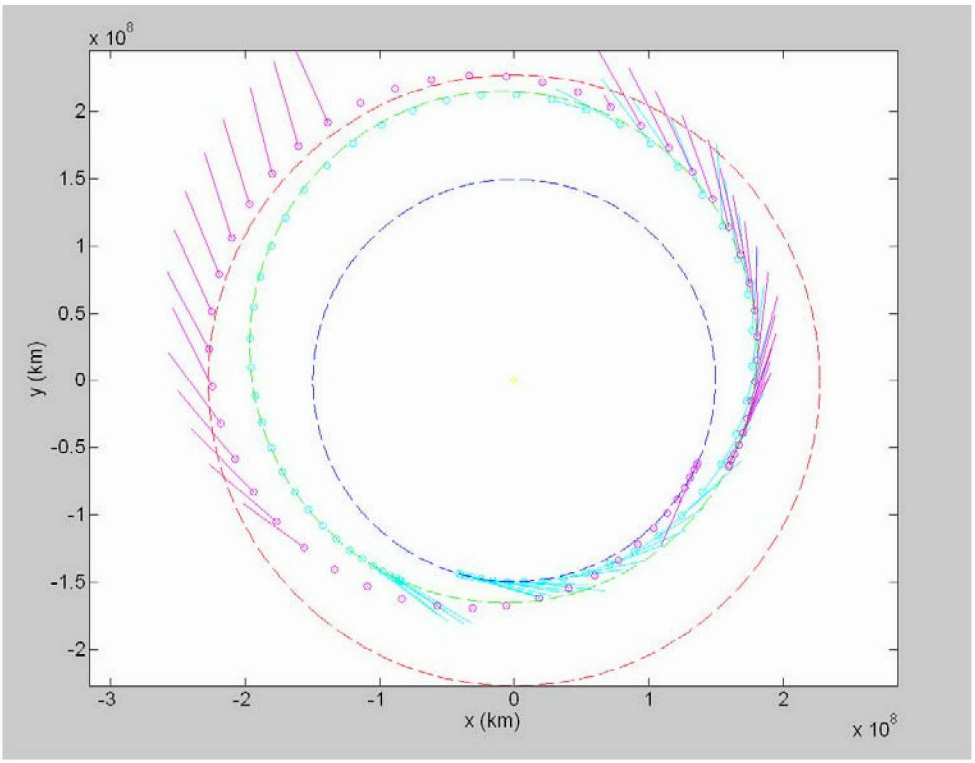

Figure 43. 47.43 N at 3006 sec (110 day surface time)

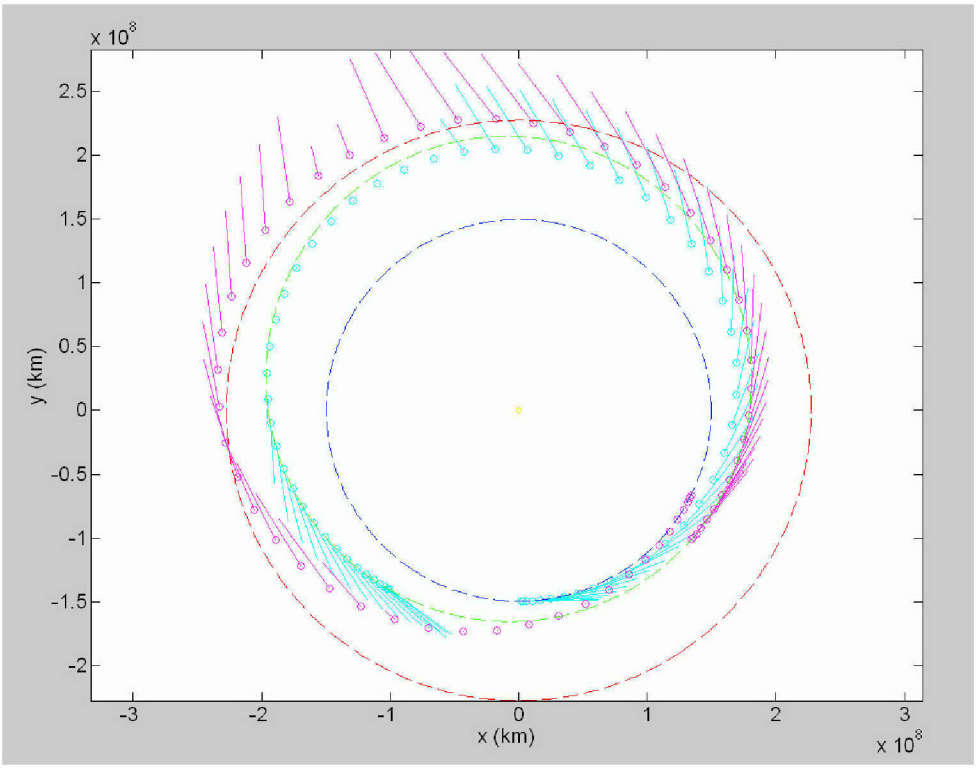

Figure 44. 35.14 N at 2821.6 sec (100 day surface time)

THIS PAGE INTENTIONALLY LEFT BLANK

V. CONCLUSIONS AND FUTURE WORK

It would appear, based on Figure 41, that fuel consumption over the course of a sample return mission optimal trajectory is a linear function of asteroid surface time; at least within the limitations of the thruster model employed here. For the assumed case, time spent on the asteroid is purchased at a cost of about 0.5 kilograms of Xenon per day. While the assumed case maybe overly conservative, similarities between it and the results shown in Figure 40 suggest that it might be a good starting point from which to extract quick rough estimates of how changes in asteroid surface time might affect fuel load. Of course, the higher the available thrust and specific impulse, the more scheduling flexibility one has in exploring the surface of 1989ML. If the spacecraft can be designed to sustain thruster performance consistent with NSTAR Throttle Level 12 (The lower line on Figure 41) over the course of the entire mission, then asteroid surface time can range from forty to one hundred and sixty days without any appreciable cost in additional fuel mass.

Furthermore, as shown in Figures 42 through 44, the optimal thrust angle trajectory for the sample return spacecraft becomes increasingly radial as thruster performance becomes increasingly constrained.

Hopefully, these insights will be of use to mission planners at JPL and elsewhere. As ion thrusters continue to proliferate, questions of optimal control will become more important and there are many aspects of the topic which need to be explored. Among these are:

Three Dimensional Orbit Transfer Models. The author has put considerable effort into formulating a MATLAB code to generate optimal low thrust trajectories in three dimensions using spherical coordinates; with little success thus far. One of the first steps in the validation process involved generating coplanar Hohmann transfers at various angles of inclination to ensure that all the results were identical. Lovely, well behaved, three dimensional coplanar transfers were generated only when available fuel mass was artificially

restricted to that quantity known to be needed for an optimal (Hohmann) transfer. Left to it's own devices by removal of the fuel mass constraint, the code generated a hideously incontinent thrust profile in which the spacecraft weaved in and out of plane in a manner than was clearly less than optimal. While the spherical dynamic equations are subject to singularities under certain circumstances, no definitive cause for the difficulties could be established at the time of this writing.

A Realistic NSTAR Thruster Model. The NSTAR thruster is likely fly on a number of different spacecraft for a long time to come. Some way of realistically coding and modeling the NSTAR throttle settings and accounting for variations in solar flux as a function of solar distance would go a long way toward increasing the fidelity of this and other models.

LIST OF REFERENCES

1. Website: http://nmp.jpl.nasa.gov/ds1/ "Deep Space 1," November 2004.

2. Website: http://www.qinetiq.com/home/markets/space/customer_leaflets.Par.0002.File.pdf "Qinetiq Highly Maneuverable Microsatellite," November 2004.

3. Website: http://www.orbitalrecovery.com/ "ConeXpress Orbital Life Extension Vehicle," November 2004.

4. Website: http://www.jpl.nasa.gov/jimo/gallery.cfm "Jupiter Icy Moons Orbiter," November 2004.

5. Website: http://www.uark.edu/misc/hera/spacecraft.html "Hera Spacecraft," November 2004.

6. Website: http://www.boeing.com/ids/edd/ep.html#30cm "Boeing 30 cm NSTAR Ion Thruster," November 2004.

7. Vallado, D. A., *Fundamentals of Astrodynamics and Applications*, Second Edition, Space Technology Library, Microcosm Press, El Segundo, CA, 2001.

8. Bryson, Arthur E., Ho, Yu-Chi, *Applied Optimal Control: Optimization, Estimation, and Control*, Hemisphere Publishing, 1975.

9. S. Josselyn, "Optimization of Low Thrust Trajectories with Terminal Aerocapture," Engineer's Thesis, U.S. Naval Postgraduate School, Monterey, CA, June 2003.

10. Brown, Charles D., *Spacecraft Mission Design*, Second Edition AIAA Education Series, American Institute for Aeronautics and Astronautics, Reston, VA, 1998.

11. Kaplan, Marshall H., *Modern Spacecraft Dynamics and Control*, John Wiley & Sons, 1976.

12. Website:http://nmp-techvalreports.jpl.nasa.gov/DS1/IPS_Integrated_Report.pdf "Ion Propulsion System (NSTAR) DS1 Technology Validation Report," November 2004.

13. I. M. Ross, *AA 3830 Class Notes*, Monterey, CA, Spring 2003.

14. Website: http://history.msfc.nasa.gov/vonbraun/recall.html "Recollections of Childhood Experiences in Rocketry as told by Wernher Von Braun 1963" November 2004.

15. I. M. Ross and F. Fahroo, "User's Manual for DIDO 2003: A MATLAB Application Package for Dynamic Optimization," *NPS Technical Report*, MAE-03-005, Department of Mechanical and Astronautical Engineering, Naval Postgraduate School, Monterey, CA September 2003

16. Website:http://www.boeing.com/defense-space/space/delta/guides.htm. "Delta II Payload Planner's Guide".November 2004.

17. Discussions between P. Croley (Former NPS Student) and the author, 2004

18. Discussions between R. Stevens (Former NPS Student) and the author, 2004

INITIAL DISTRIBUTION LIST

1. Defense Technical Information Center
   Ft. Belvoir, Virginia

2. Dudley Knox Library
   Naval Postgraduate School
   Monterey, California

3. Professor I. Michael Ross
   Naval Postgraduate School
   Monterey, California

4. Stacy Weinstein
   Jet Propulsion Laboratory
   Pasadena, California

5. Jack W. Rust
   SPAWAR (PMW 146)
   San Diego, California